



This is to certify that the

thesis entitled

THE ROLE OF MONOVALENT CATIONS IN THE ACTIVATION OF TRYPTOPHANASE: A SPECTRO-SCOPIC AND KINETIC STUDY

presented by

Barbara Kennedy

has been accepted towards fulfillment of the requirements for

Ph.D. degree in Biophysics

M. A. El-Bayoumi Major professor

Date October 9, 1979

O-7639

羽内ドラリ



OVERDUE FINES ARE 25¢ PER DAY PER ITEM

Return to book drop to remove this checkout from your record.

THE ROLE OF MONOVALENT CATIONS IN THE ACTIVATION OF TRYPTOPHANASE: A SPECTROSCOPIC AND KINETIC STUDY

Ву

Barbara Kennedy

A DISSERTATION

Submitted to

Michigan State University

in partial fulfillment of the requirements

for the degree of

DOCTOR OF PHILOSOPHY

Department of Biophysics

ABSTRACT

THE ROLE OF MONOVALENT CATIONS IN THE ACTIVATION OF TRYPTOPHANASE: A SPECTROSCOPIC AND KINETIC STUDY

By

Barbara Kennedy

Tryptophanase is a pyridoxal-5°-phosphate enzyme which requires activating monovalent cations in order to catalyze the \checkmark , β -elimination reaction

Different effects on the absorption spectrum of holotryptophanase are known for potassium, in which case there are two pH dependent bands at 337 nm and 420 nm, and for sodium, in which case there is only a 420 nm band.

In this study we have examined the effect of monovalent cations and tetramethylammonium and phosphate ions on the absorption spectrum of holotryptophanase. Ammonium, potassium, and rubidium strongly activate the enzyme and also promote the appearance of the 337 nm band, whereas in the case of lithium, cesium, or sodium the 420 nm band predominates and the enzyme activity is low. The 337 nm band is decreased in buffers containing tetramethylammonium ion and enhanced in buffers containing phosphate ion.

Comparison of the fluorescence spectrum of apotryptophanase, $\lambda_{\rm ex}^{=}$ 280 nm, with the fluorescence spectrum of holotryptophanase, $\lambda_{\rm ax}^{=}$ 280 nm,

leads to the conclusion that the 337 nm absorbing form of bound pyridoxal-5°-phosphate is excited by nonradiative energy transfer from the tryptophan residues of the protein and in turn emits at about 400 nm.

A 510 nm emission arises from the 420 nm absorbing form of bound pyridoxal-5°-phosphate which is created in the excited state by an intermolecular proton transfer. Departures of the ratio of the 400 nm to 510 nm emissions from the ratio of the 337 nm to 420 nm absorptions may indicate specific effects of monovalent cations on the excited state proton transfer reaction. Analysis of fluorescence decay data in order to prove this mechanism is complicated by the presence of short, close-together lifetimes.

In rapid-scanning stopped flow kinetics experiments involving changes of pH or monovalent cations, we have observed a slow process, seconds in duration, in which a 420 nm absorber disappears and a 337 nm absorber appears, or vice versa. We have interpreted this observation as a protonation-deprotonation reaction coupled to conformational change in the protein. A still slower process may involve the interconversion of the holoenzyme and the apoenzyme.

ACKNOWLEDGMENTS

I would like to thank Dr. M. Ashraf El-Bayoumi for his friendship and guidance during the course of this work, Drs. Clarence H. Suelter and James L. Dye for their support of this project, and my graduate student colleagues in the enzyme group for their help and advice.

I also wish to express my appreciation to Dr. Estelle J. McGroarty for six years of friendship and assistance. I am especially grateful to Robin Fink for helping me to complete this work and for illustrating this dissertation.

For encouragement, thanks to Nina, Vicki, Ann, Billie, Barbara, Sharmila, Soheir, Jocelyne, Denise, Rene, Cindy, Myra, and Rachael.

TABLE OF CONTENTS

Chapter 1.	Absorption and emission properties of	
	B ₆ compounds	1
	A. Introduction	1
	B. Absorption properties	3
	C. Emission properties	13
Chapter 2.	Structure and function of B6 enzymes	18
	A. General properties of B ₆ enzymes	18
	B. Aspartate aminotransferase	22
	C. Glycogen phosphorylase	29
	D. Tryptophanase	32
Chapter 3.	An hypothesis regarding the role of	
	monovalent cations in tryptophanase	40
Chapter 4.	Results and discussion	45
	A. Absorption and emission studies	45
	B. Fluorescence lifetime studies	66
	C. Kinetic studies	74
Chapter 5.	Materials and methods	81
	A. Growth of E. coli B/1t7a	81
	B. Preparation of the Sepharose column	83
		83 84
	B. Preparation of the Sepharose column	_

F. Enzyme assay of tryptophanase	89
G. Spectral measurements	89
H. Rapid-scanning stopped flow kinetics	
measurements	92
Chapter 6. Future work	94
Bibliography	98

LIST OF TABLES

Table 1.	Activating constants for monovalent cations 33	36
Table 2.	Concentrations of cations	54
Table 3.	Lamp shift corrections	70
Table 4.	Decay parameters	72
Table 5.	Decay parameters with lamp shifted	72

LIST OF FIGURES

Figure 1.	B ₆ compounds 1	1
Figure 2.	Ionic and tautomeric forms of a B6	
	Schiff's base ³	3
Figure 3.	Quinonoid structure of a B ₆ Schiff's base ³	4
Figure 4.	3-hydroxy-4-formylpyridine Schiff's base 6	6
Figure 5.	Pyridoxal-P aldehyde and hydrate 11	8
Figure 6.	Absorption spectra of pyridoxal-P	
	as a function of pH11	10
Figure 7.	Absorption spectra of pyridoxal-P hydrate 11	11
Figure 8.	Absorption spectra of pyridoxal-P aldehyde 11	11
Figure 9.	Ground state (left) and excited state 14	12
Figure 10.	Fluorescence spectra of pyridoxal-P hydrate 15	14
Figure 11.	Fluorescence spectra of pyridoxal-P aldehyde 15	14
Figure 12.	Excited state proton transfer scheme 19	16
Figure 13.	Reactions of B enzymes 1	18
Figure 14.	Schiff's base with substrate amino acid ²²	19
Figure 15.	Quinonoid intermediate 22	20
Figure 16.	Protonation at the formyl carbon 22	21
Figure 17.	Products of transamination 22	21
Figure 18.	362 and 426 nm forms of aspartate	
	aminotransferase 24	22
Figure 19.	Pyridoxal-P Schiff's base in solution and enzyme	24

Figure 20.	Reactants for nucleophilic addition 24	25
Figure 21.	Formyl carbon bonded tetrahedrally 24	27
Figure 22.	Active site of aspartate aminotransferase 17	28
Figure 23.	Pyridoxal-P Schiff's base micelle 7,8	31
Figure 24.	Absorption spectra of tryptophanase	
	as a function of pH ²⁹	32
Figure 25.	Absorption spectra of tryptophanase	
	as a function of cation ²⁹	33
Figure 26.	Mechanism of action of tryptophanase 29	34
Figure 27.	Possible 337 rm forms	41
Figure 28.	Analogous coenzyme forms	42
Figire 29.	Absorption and difference absorption spectra	46
Figure 30.	Pyridoxal-P binding reaction	46
Figure 31.	Fluorescence spectrum of apotryptophanase	48
Figure 32.	Absorption spectra of tryptophanase in TMA	48
Figure 33.	Tryptophanase absorption spectra	51
Figure 34.	Absorption spectrum of holotryptophanase-	
	L-ethionine	52
Figure 35.	Fluorescence spectrum of holotryptophanase	53
Figure 36.	Absorption spectra in ammonium,	
	potassium, rubidium	55
Figure 37.	Absorption spectra in sodium,	
	lithium, cesium	55
Figure 38.	Absorption spectra in ammonium	56
Figure 39.	Absorption spectra in potassium	57
Figure 40.	Absorption spectra in rubidium	57
Figure 41.	Fluorescence spectrum of buffer	59

Figure 42.	Fluorescence spectrum of tryptophanase	
	in ammonium	59
Figure 43.	Fluorescence spectrum of tryptophanase	
	in potassium	60
Figure 44.	Fluorescence spectrum of tryptophanase	
	in rubidium	60
Figure 45.	Fluorescence spectrum of tryptophanase	
	in lithium	61
Figure 46.	Fluorescence spectrum of tryptophanase	
	in cesium	61
Figure 47.	Fluorescence spectrum of tryptophanase	
	in sodium	62
Figure 48.	Fluorescence spectra of tryptophanase	
	in potassium	62
Figure 49.	Fluorescence decay of 9-cyanoanthracene	69
Figure 50.	Fluorescence decay of tryptophanase, 420 nm	71
Figure 51.	Fluorescence decay of tryptophanase, 510 nm	71
Figure 52.	pH drop and pH jump ⁵³	
Figure 53.	Absorbance-wavelength-time surface	78
Figure 54.	First and last spectra	78
Figure 55.	Time cut at 337 nm	7 9
Figure 56.	Time cut at 420 mm	79
Figure 57.	Pyridoxal-P binding to anotryptophanase	80

CHAPTER 1

ABSORPTION AND EMISSION PROPERTIES OF B COMPOUNDS

A. INTRODUCTION

Vitamin B_6 is the name given to pyridoxal-5'-phosphate (pyridoxal-P) and related compounds including pyridoxal, pyridoxol, and pyridoxal-mine. The biologically active form of Vitamin B_6 is pyridoxal-P which is bound to a variety of enzymes as a Schiff's base with an E-amino group of a lysine residue. ¹

Figure 1. B₆ compounds ¹

The spectroscopic characteristics of B₆ enzymes are essentially those of the pyridoxal-P Schiff's base in the environment provided by the active site of the enzyme. The pyridoxal-P Schiff's base exists in several ionic forms as well as displaying prototropic tautomerism in which a proton can move between the pyridine nitrogen and the imine nitrogen. Such prototropic equilibria involving heteroatoms usually have activation energy that is low enough for the rates of the tautomeric reactions to be fast and for the tautomers to be in mobile equilibrium in solution. Furthermore, because of these low energy differences, tautomeric equilibrium constants are very sensitive to environmental effects, in particular to solvent, concentration, and temperature. Therefore, when analyzed with these facts in mind, the spectra of B₆ enzymes may yield information about conditions and changes of conditions at the active site of the enzyme.

The B₆ coenzyme is thought to participate in the mechanism of catalysis in an intimate way, including the formation of a covalent linkage with the substrate amino acid to give other pyridoxal-P Sciff's bases at the active site of the enzyme. In their review article on heteroaromatic tautomerism² El Guero et al. emphasize the importance of depicting reaction mechanisms in their correct ionic and tautomeric forms. The spectra of B₆ enzymes and the products of their reactions with substrates, inhibitors, and other molecules can provide information which can assist in assigning correct ionic and tautomeric forms in the mechanisms of action of these enzymes.

B. ABSORPTION PROPERTIES

Johnson and Metzler³ review the spectral data on B₆ compounds and discuss the methodology for resolving the spectra of the various ionic and tautomeric forms. They discuss the B₆ spectra in terms of the three $\pi - \pi^{\#}$ transitions of benzene. Spectral variations of the structures in Figure 2 can be explained by considering the energies of locally excited benzene states (L.E.) and charge transfer states (C.T.). In the latter, the OH and O groups act as the electron donor and the azomethine group acts as the electron acceptor.⁴ One must bear in mind that the description of a state as being C.T. or L.E. is correct only in the zeroth order approximation and that interactions of C.T. and L.E. states must be considered in order to account for the energies and intensities of the observed absorption bands.

Figure 2. Ionic and tautomeric forms of a B Schiff's base 3

One may then consider the first absorption band in these three compounds to arise from a transition to a C.T. state mixed with the lowest L.E. state of benzene. The larger ionization energy of OH as compared to 0 would explain the shorter wavelength of the band of compound I as compared to compound II. The larger electron affinity of a protonated azomethine group would explain the longer wavelength absorption of compound III. Using valence bond theory language one would state that the quinonoid structure (Figure 3) has a major contribution in compound III, while in compound II it has a smaller contribution and in compound I it has practically no contribution.

Figure 3. Quinonoid structure of a B Schiff's base 3

A second factor that may affect the position of the first absorption band is a rotation about the bond between the phenyl ring and the azomethine group. In general, the more planar the system the greater will be the amount of conjugation and the longer the wavelength of the absorption maximum. Johnson and Metzler³ use this possibility in

explaining the anomalous values for the absorption maximum of the decompyridoxal-leucine Sciff's base. The pK_{a} values are also anomalous for this compound: 11.7 and 6.5 for the imine and pyridine nitrogens, respectively, as compared to more typical values of 10.5 and 5.9.

In a recent abstract, Metzler et al.⁵ report that they have measured the electronic absorption spectra of the individual ionic and tautomeric forms of Schiff's bases of pyridoxal-P, as well as determining the pk values. Spectra were resolved by assuming lognormal distribution curves.

A very complete assignment of spectral maxima to the molecular species of B₆ Schiff's bases with methyl valinate and n-butylamine is given by Karube and Matsushima. Figure 4 summarizes the assignments for the longest wavelength band of the Schiff's base of 3-hydroxy-4-formyl-pyridine. The spectra of the corresponding forms for pyridoxal-P are at longer wavelengths by less than 10 nm. It is particularly interesting to note that the Schiff's base of pyridoxal-P with methyl valinate in neutral methanol absorbs at 340 nm, with a shorter wavelength maximum at 254 nm. Presumably these absorptions arise from a form like compound II of Figure 4. The Schiff's base of pyridoxal-P with n-butylamine absorbs at 418, 336, 288, and 272 nm. In this case, there is an equilibrium between forms like II and III in Figure 4. Also, more polar solvents favor the more polar form III. In neutral water, however, a dipolar form IV would be expected to predominate but it is not stable.

The absorption properties of the Schiff's base formed between n-dodecylamine and pyridoxal-P are studied by Gani et al. 7,8 N-dodecylamine was shown to form mixed micelles with CetMe_NBr with the pyridoxal-P bound in 1:1 stoichiometry to the n-dodecylamine. The complex absorbs

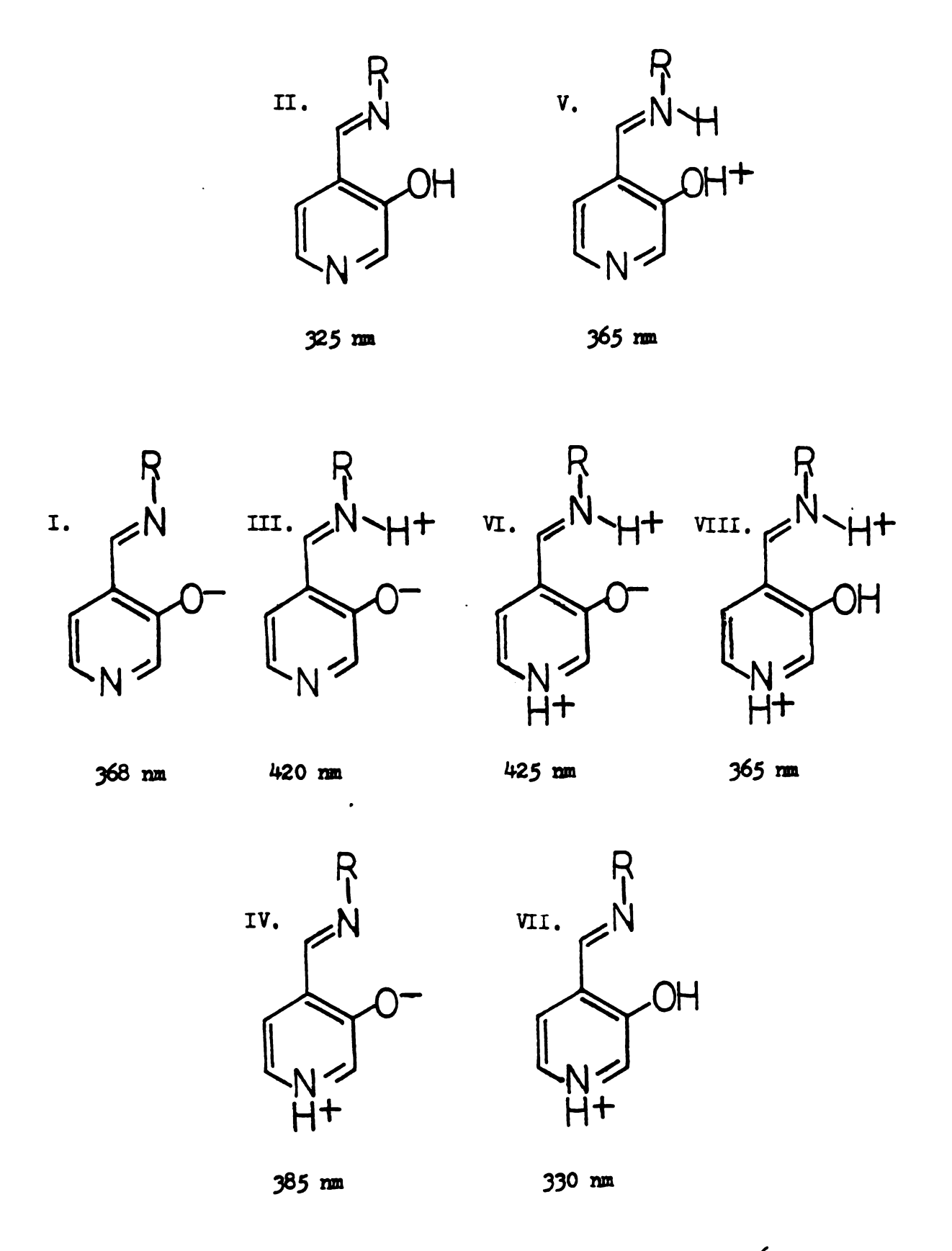


Figure 4. 3-hydroxy-4-formylpyridine Schiff's base 6

at 333 nm and 250 nm with a minor peak at 415 nm. Gani et al. attribute the spectrum to an enclimine structure embedded in a hydrophobic environment.

Pyridoxal Schiff's bases of poly (L- < amino acids) are studied by Dentini et al. At pH 7 in water/methanol solutions the pyridoxylidene-imine group absorbs at 420, 335, 253, and 210 nm, with a blue shift in the 335 nm band with increasing ratio of water to methanol. The authors suggest a Schiff's base linkage to one amino acid residue together with a partially electrostatic hydrogen bond between the nearest NH₃⁺ group and the phenolic oxygen.

Conformational analysis of Schiff's bases of pyridoxal with alanine, valine, leucine, and phenylalanine are carried out by Weintraub et al. 10 All four Schiff's bases had an energy minimum corresponding to a planar conformation with the carbonyl carbon, \propto -carbon, and nitrogen in the plane of the pyridine ring. In addition, phenylalanine, alanine, and leucine had an energy minimum in which the $C_{\rm ex}$ -N bond was rotated so that the H, R, or COO group was perpendicular to the plane of the pyridine ring. The population of the latter conformer ranged from 1% for phenylalanine to 17 % for alanine.

Morosov et al. 11 utilize the method of least squares in order to calculate the absorption spectra of the individual forms of pyridoxal-P. Pyridoxal-P is assumed to exist in three ionic forms of each an aldehyde and a hydrate, the latter of which is formed by a hydrogen ion catalyzed nucleophilic attachment reaction. The reactivity of the carbonyl group is a maximum when the pyridine nitrogen is protonated so that the equilibrium shifts towards the aldehyde forms as the pH increases. Significant amounts of the appropriate ionic forms of the hydrate and of

Figure 5. Pyridoxal-P aldehyde and hydrate 11

the aldehyde are shown to exist at neutral pH. Ionic strength of the solution does not change the spectra of the forms but with increasing ionic strength the hydrate/aldehyde ratio is increased. Ionization of the phosphate group seems to have little effect on the absorption spectra of the forms of pyridoxal-P. Morosov et al.'s spectra are shown in Figures 6, 7, and 8.

Harris et al. 12 evaluate the electronic absorption spectra of the individual forms of pyridoxal-P by a spectral resolution using lognormal curves. In order to obtain a good fit of their data they require an additional form to be present, an uncharged tautomer of the dipolar aldebyde form. Apparent pk values of 3.62 and 8.33 are reported for the phenolic group and the pyridine nitrogen, respectively.

Savin et al. ¹³ calculate the π -electronic structures and absorption spectra of B_6 compounds by the semiempirical Pariser-Parr-Pople method. Substituents to the parent compound 3-hydroxypyridine have a weak effect on the absorption spectrum with the exception of the carbonyl group substituted in the 4 position. In the last case, it is determined that the longest wavelength band is associated, in the lowest approximation, with the transition of the electron from the upper filled orbital of the ring to the antibonding orbital of the carbonyl group. In all cases upon transition to the lowest excited singlet state there occurs an increase of the π -electronic charge on the pyridine nitogen and a large decrease on the phenolic oxygen (Figure 9). On the basis of a more elaborate calculation, Bashulina et al. ¹⁴ report that upon excitation to the lowest excited singlet state a transfer of π -electronic charge amounting to 0.3 to 0.5 electron charges takes place from the pyridine ring and the phenolic group to the carbonyl group.

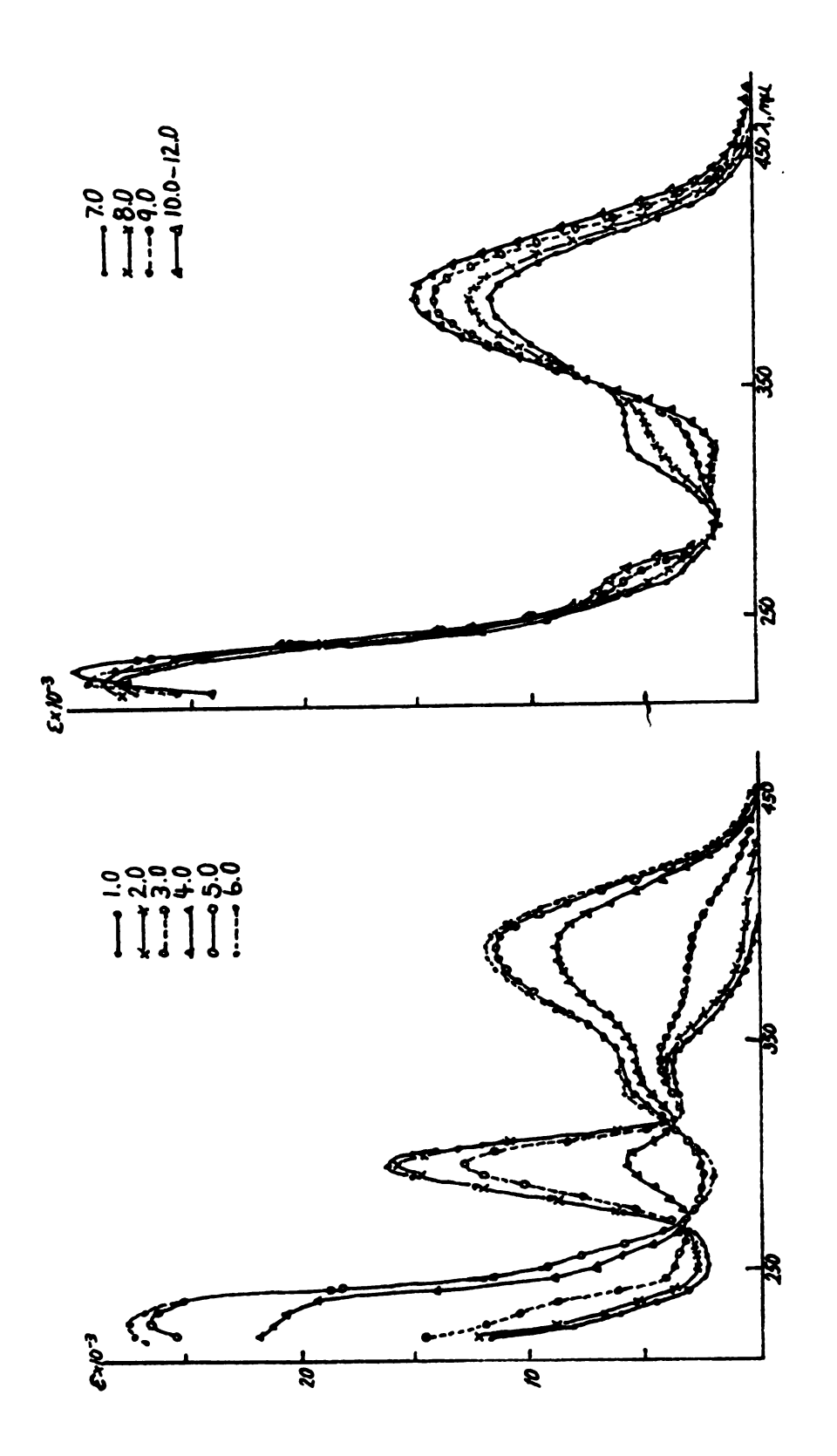


Figure 6. Absorption spectra of pyridoxal-P as a function of pH^{11}

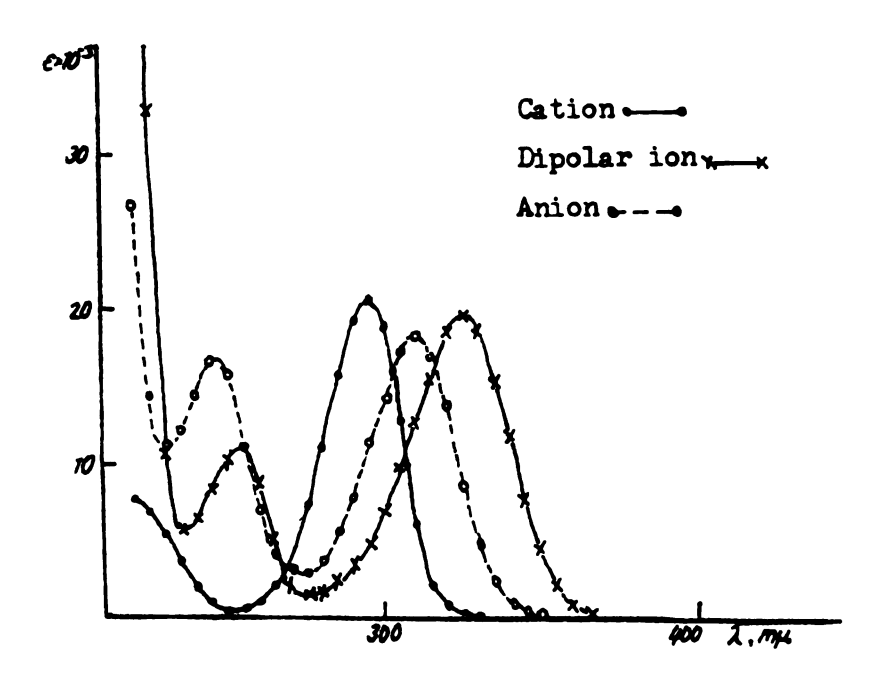


Figure 7. Absorption spectra of pyridoxal-P hydrate 11

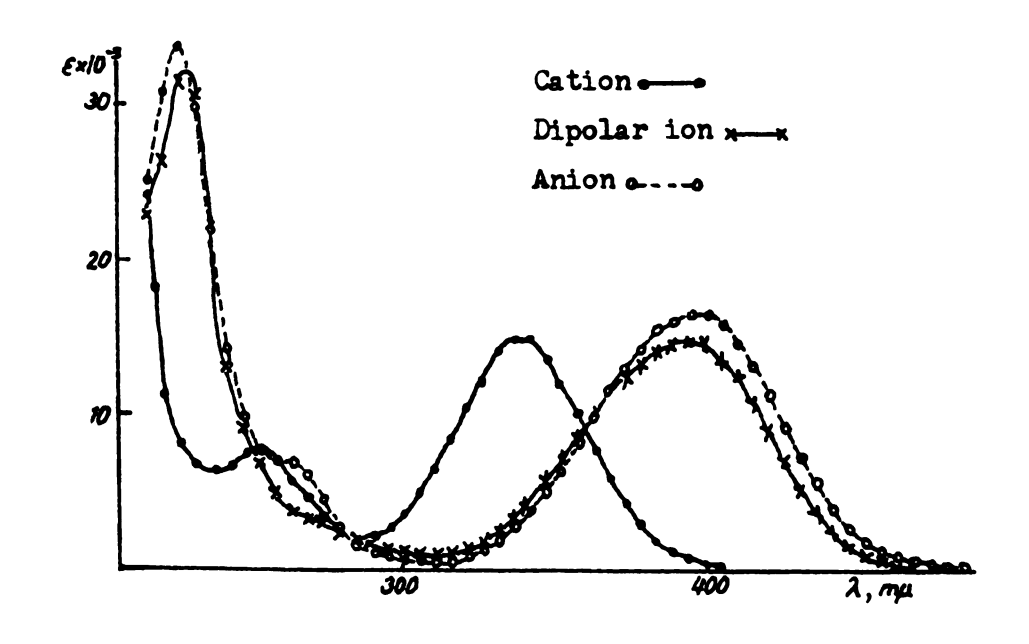


Figure 8. Absorption spectra of pyridoxal-P aldehyde 11

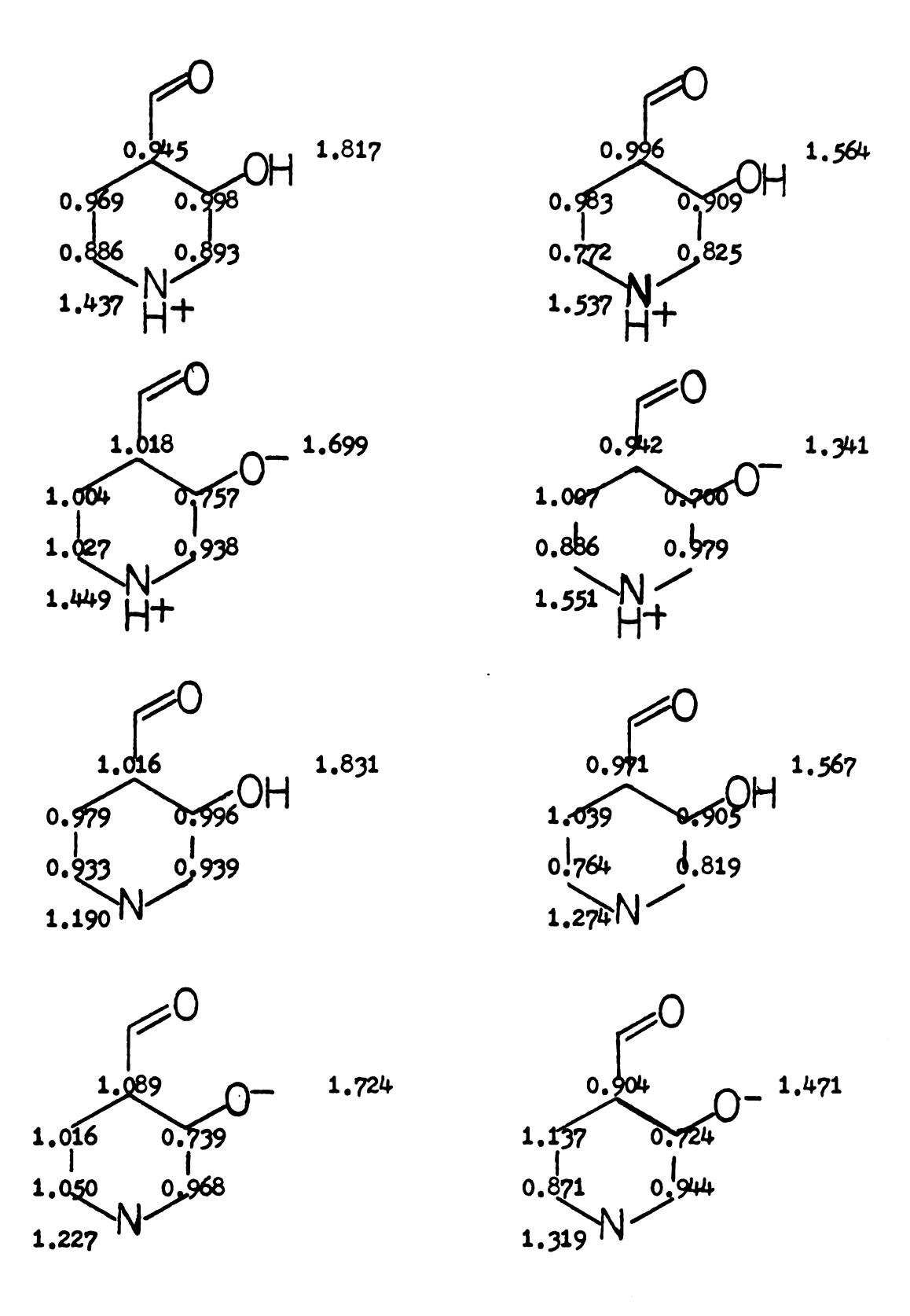


Figure 9. Ground state (left) and excited state 14

C. EMISSION PROPERTIES

Morosov et al. 15 present the fluorescence spectra of the different forms of pyridoxal-P as resolved by the method of least squares. The hydrate cation has an excited state ionization associated with a sharp reduction in the pK_a^* of the phenolic group; emission is then observed from the dipolar ion. Shifts to shorter wavelengths of about 20 mm are attributed to the ionization of the phosphate hydroxls and the pyridine nitrogen. Stokes shifts are reported to be 55 to 70 mm.

In the aldehyde, dissociation of the pyridine nitrogen and the phosphate hydroxyls lead instead to a shift to longer wavelengths of about 40 nm. The Stokes shifts are 115 to 150 nm. The latter fact is explained by the authors by the formation of an intramolecular hydrogen bond in the excited state at all pH values.

Bridges et al. ¹⁶ define the Stokes shift as the difference between the wave number of the longest wavelength of the excitation maximum and that of the shortest wavelength of the fluorescence maximum and they state that the Stokes shift is a measure of the energy required to raise the compound to the first excited state. They report Stokes shifts of 9.36, 5.86, 5.50, and 5.76 kK for the cation, dipolar ion, neutral form, and anion, respectively. In addition they give values of the Stokes shift for many B₆ compounds and they conclude that for cations ionizing in the excited state one should expect 8 to 10 kK as compared to 4 to 6 kK for other forms not exhibiting excited state ionizations.

From values for absorption and emission maxima of pyridoxal-P given by Morosov et al. 15 one can estimate the Stokes shifts for the pyridoxal-P aldehyde to be 7.2, 5.6, and 7.1 kK for the cation, dipolar ion, and

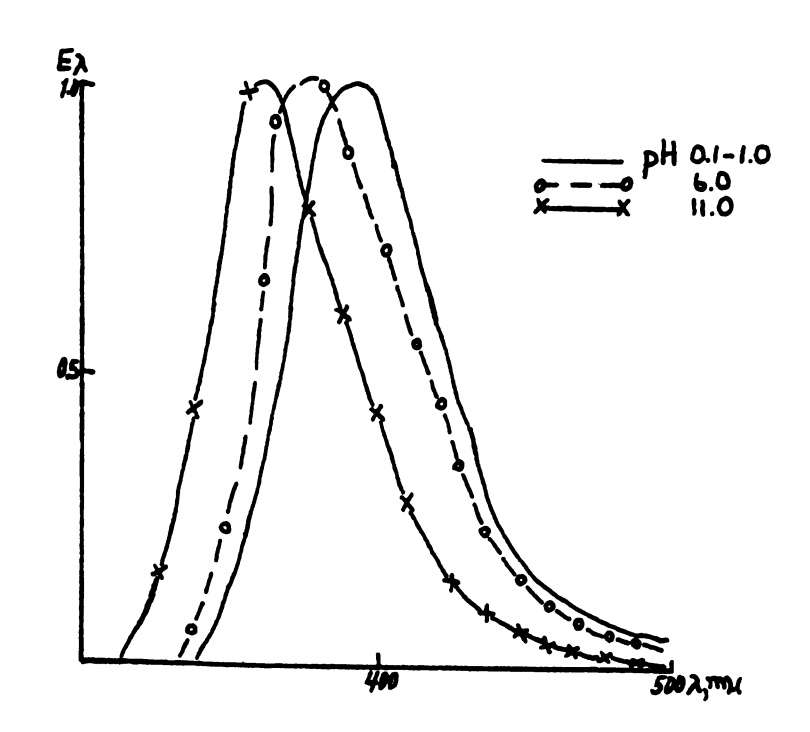


Figure 10. Fluorescence spectra of pyridoxal-P hydrate 15

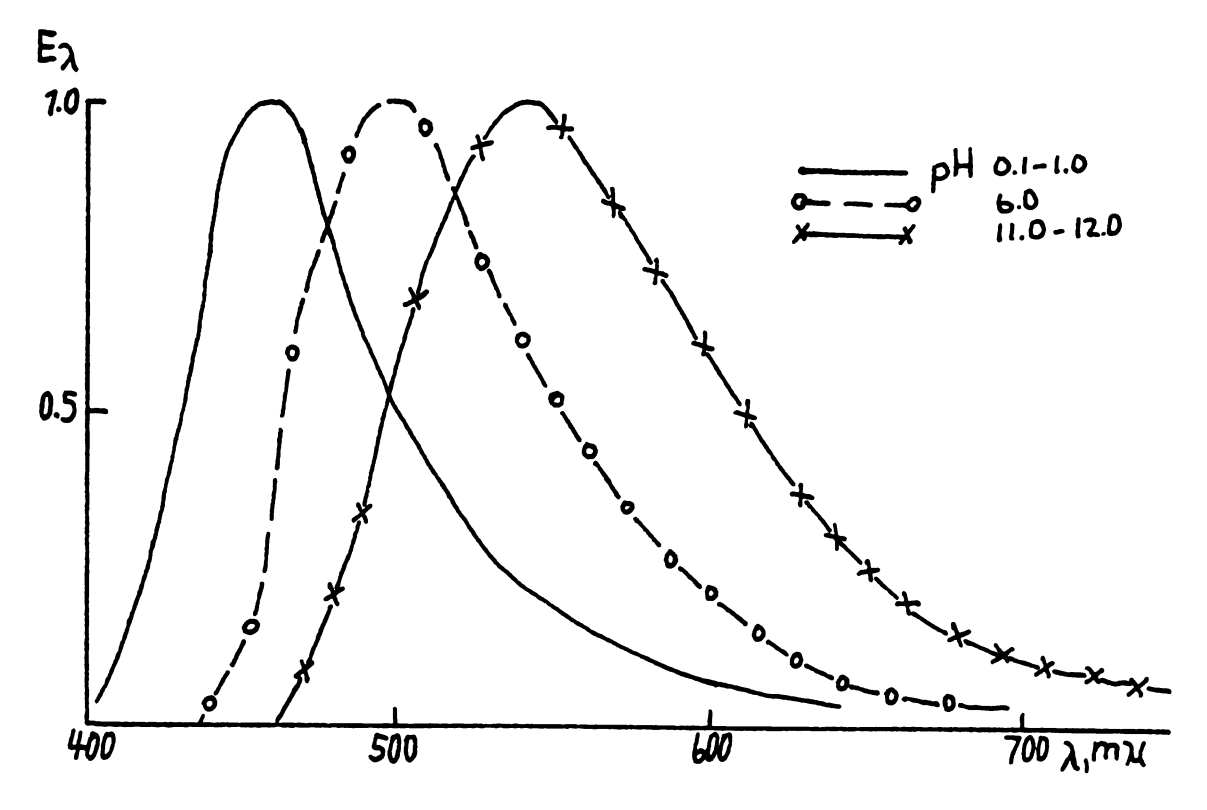


Figure 11. Fluorescence spectra of pyridoxal-P aldehyde 15

anion, respectively. Based on the results of Bridges et al., excited state proton transfer cannot be inferred from these values alone. In substituted benzene molecules it is known that a large transfer of π -electronic charge toward the carbonyl groups and away from the phenolic groups occurs upon excitation (a fact that is responsible for the increase in the pK_a of the carbonyl group and the decrease in the pK_a of the phenolic group that sometimes leads to proton transfer in the excited state). It may be that the interaction with the surrounding medium is changed sufficiently in passing to the excited state to explain the magnitude of the Stokes shifts that are observed.

Fluorescence lifetimes of less than one nanosecond and very low quantum yields are reported by Morosov et al. ¹⁵ They argue that these observations support the excited state intramolecular hydrogen bonding hypothesis.

Arrio-Dupont studies the Schiff's base of pyridoxal-P and n-butyl-amine. 17 This compound absorbs at 340 and 408 nm in water and emits at 400 and 505 nm corresponding to the two absorptions. She measured the pK of the imine nitrogen to be 11.5 and calculated the pK by Weller's method 18 to be 12.4. Protonation of the pyridine nitrogen does not change the absorption spectrum but fluorescence intensity is enhanced twentyfold. In a pyridoxal-valine Schiff's base the pK of the imine nitrogen was determined to be 8.5 with the pyridine nitrogen protonated as compared to 10.4 if it is not protonated.

In nonaqueous solvents the 340 nm absorbing species shows a second emission at 525 nm; the Stokes shift is greater than 10 kK. 19 Arrio-Dupont proposes an excited state proton transfer scheme shown in Figure 12 to explain the two emissions. In nonpolar solvents the equilibrium

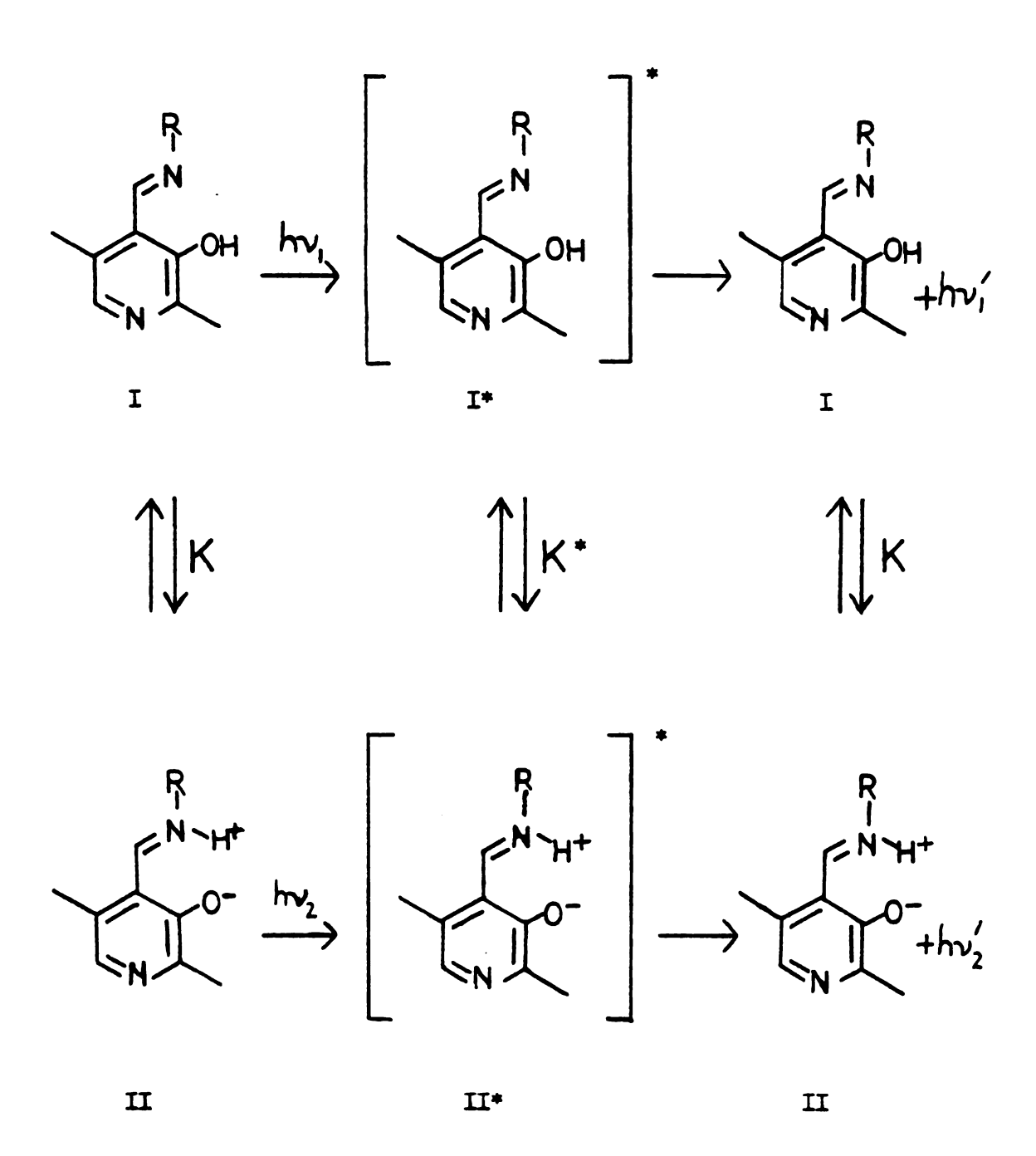


Figure 12. Excited state proton transfer scheme 19

is displaced toward II* whereas in H accepting solvents the equilibrium is shifted toward I* · · · · solvent.

Additional proof for the proton transfer mechanism is given by Veinberg et al. 20,21 in a study of Schiff's bases of hexylamine with salicylaldehyde and o-methylsalicylaldehyde. The 535 nm emission observed in CCl₁ in the case of salicylaldehyde is not observed in the case of o-methylsalicylaldehyde because the presence of a methyl group instead of a proton makes proton transfer impossible.

CHAPTER 2

STRUCTURE AND FUNCTION OF B ENZYMES

A. GENERAL PROPERTIES OF B ENZYMES

Pyridoxal-P is the coenzyme of a number of enzymes involved in the reactions of amino acid metabolism. Several classes of reactions catalyzed by these enzymes are shown in Figure 13.

Figure 13. Reactions of B₆ enzymes¹

The coenzyme is linked covalently to the enzyme by a condensation reaction of the pyridoxal-P carbonyl group with the £-amino group of a lysine residue in the enzyme active site:

A general mechanism for pyridoxal-P catalyzed reactions has been proposed independently by Snell and by Braunstein and presented concisely by Pullman and Pullman.²² For purposes of their presentation, the ionic and tautomeric forms of the pyridoxal-P are chosen arbitrarily. In addition, the effects of metal cations and of the 5° phosphate group are disregarded. In the first step, the enzyme bound Schiff's base (or imine or azomethine) is converted to a Schiff's base with a substrate amino acid by a transimination reaction.

22

The second step requires labilization of the H, COO, or R group attached to the c-carbon. The driving force for this reaction is found in the gain of resonance energy upon formation of the quinonoid intermediate, shown in Figure 15 for the case of labilization of the -hydrogen.

$$\begin{array}{c} \mathbb{R} & \mathbb{R} & \mathbb{R} \\ \mathbb{R} & \mathbb{R} & \mathbb{R} & \mathbb{R} & \mathbb{R} \\ \mathbb{R} & \mathbb{R} & \mathbb{R} & \mathbb{R} & \mathbb{R} \\ \mathbb{R} & \mathbb{R} & \mathbb{R} & \mathbb{R} & \mathbb{R} \\ \mathbb{R} & \mathbb{R} & \mathbb{R} & \mathbb{R} & \mathbb{R} \\ \mathbb{R} & \mathbb{R} & \mathbb{R} & \mathbb{R} & \mathbb{R} \\ \mathbb{R} & \mathbb{R} & \mathbb{R} & \mathbb{R} & \mathbb{R} \\ \mathbb{R} & \mathbb{R} & \mathbb{R} & \mathbb{R} & \mathbb{R} \\ \mathbb{R} & \mathbb{R} & \mathbb{R} & \mathbb{R} & \mathbb{R} \\ \mathbb{R} & \mathbb{R} & \mathbb{R} & \mathbb{R} & \mathbb{R} \\ \mathbb{R} & \mathbb{R} & \mathbb{R} & \mathbb{R} & \mathbb{R} \\ \mathbb{R} & \mathbb{R} & \mathbb{R} & \mathbb{R} & \mathbb{R} \\ \mathbb{R} & \mathbb{R} & \mathbb{R} & \mathbb{R} & \mathbb{R} \\ \mathbb{R} & \mathbb{R} & \mathbb{R} & \mathbb{R} & \mathbb{R} \\ \mathbb{R} & \mathbb{R} & \mathbb{R} & \mathbb{R} & \mathbb{R} \\ \mathbb{R} & \mathbb{R} & \mathbb{R} & \mathbb{R} & \mathbb{R} \\ \mathbb{R} & \mathbb{R} & \mathbb{R} & \mathbb{R} & \mathbb{R} \\ \mathbb{R} & \mathbb{R} & \mathbb{R} & \mathbb{R} & \mathbb{R} \\ \mathbb{R} & \mathbb{R} & \mathbb{R} & \mathbb{R} & \mathbb{R} \\ \mathbb{R} & \mathbb{R} & \mathbb{R} & \mathbb{R} & \mathbb{R} \\ \mathbb{R} & \mathbb{R} & \mathbb{R} & \mathbb{R} \\ \mathbb{R} & \mathbb{R} & \mathbb{R} & \mathbb{R} & \mathbb{R} \\ \mathbb{R} & \mathbb{R} & \mathbb{R} & \mathbb{R} & \mathbb{R} \\ \mathbb{R} & \mathbb{R} & \mathbb{R} & \mathbb{R} & \mathbb{R} \\ \mathbb{R} & \mathbb{R} & \mathbb{R} & \mathbb{R} & \mathbb{R} \\ \mathbb{R} & \mathbb{R} & \mathbb{R} & \mathbb{R} & \mathbb{R} \\ \mathbb{R} & \mathbb{R} & \mathbb{R} & \mathbb{R} & \mathbb{R} \\ \mathbb{R} & \mathbb{R} & \mathbb{R} & \mathbb{R} & \mathbb{R} \\ \mathbb{R} & \mathbb{R} & \mathbb{R} & \mathbb{R} & \mathbb{R} \\ \mathbb{R} & \mathbb{R} & \mathbb{R} & \mathbb{R} & \mathbb{R} & \mathbb{R} \\ \mathbb{R} & \mathbb{R} & \mathbb{R} & \mathbb{R} & \mathbb{R} & \mathbb{R} \\ \mathbb{R} & \mathbb{R} & \mathbb{R} & \mathbb{R} & \mathbb{R} & \mathbb{R} \\ \mathbb{R} & \mathbb{R} & \mathbb{R} & \mathbb{R} & \mathbb{R} & \mathbb{R} \\ \mathbb{R} & \mathbb{R} & \mathbb{R} & \mathbb{R} & \mathbb{R} & \mathbb{R} \\ \mathbb{R} & \mathbb{R} \\ \mathbb{R} & \mathbb{R} & \mathbb{R} & \mathbb{R} & \mathbb{R} & \mathbb{R} \\ \mathbb{R} & \mathbb{R} \\ \mathbb{R} & \mathbb{R} \\ & \mathbb{R} \\ & \mathbb{R} \\ & \mathbb{R} & \mathbb{R$$

Figure 15. Quinonoid intermediate 22

Following the labilization step is a protonation at the formyl carbon in the case of transamination as shown in Figure 16 or a protonation at the α -carbon in the case of racimization, decarboxylation, or α, β -elimination. Finally the C=N bond is hydrolyzed. The products formed at this stage may undergo further reaction and are shown in Figure 17 for the transamination reaction.

Pullman and Pullman²² state: "... as concerns the metal ions which participate in the nonenzymic reactions, they are considered as models of the functions played by the apoenzymes of pyridoxal-phosphate proteins. Their activating action is postulated to occur through the formation of reactive chelated intermediates...the formation of metal chelates may influence favorably the reaction scheme by an appropriate direct electronic influence on the charge distribution and by its contribution to the maintenance of coplanarity between the pyrimidine ring of the pyridoxal and the external groups. This last effect has the double result of stabilizing the system and facilitating the W-electronic displacements involved in the mechanism of action of the coenzyme."

Figure 16. Protonation at the formyl carbon

Figure 17. Products of transamination

B. ASPARTATE AMINOTRANSFERASE

Aspartate aminotransferase catalyzes the reaction 1

L-aspartic acid + o(-ketoglutaric acid

oxaloacetic acid + L-glutamic acid

The absorption spectrum of aspartate aminotransferase has a major peak near 280 nm corresponding to the absorption of the aromatic amino acid residues of the protein. 24 Peaks at 362 and 426 nm are attributed to the absorption of the coenzyme pyridoxal-P which is bound to a lysine residue of the protein in a Schiff's base linkage. The 426 nm form predominates at low pH and is converted to the 362 nm form as the pH is raised, with a pK of 6.2 for the transition.

Ivanov and Karpeisky²⁴ cite evidence from the fluorescence studies of Fasella⁶⁸ that suggests a dipolar form for the 362 nm form of the coenzyme, with protonated pyridine nitrogen and deprotonated imine nitrogen. The 426 nm form appears upon protonation at the imine nitrogen.

$$\mathbb{P} \xrightarrow{N} \mathbb{Q}^{-}$$

Figure 18. 362 and 426 nm forms of aspartate aminotransferase²⁴

According to Ivanov and Karpeisky²⁴ the coenzyme is attached non-covalently to the enzyme at the phosphate group and the methyl group, as well as the pyridine nitrogen being hydrogen bonded to a tyrosine residue of the protein. This last attachment is inferred from the presence of a negative band with extremum at 295-300 nm in the circular dichroism spectrum of holoaspartate aminotransferase which is absent in the spectrum of the apoenzyme. The authors claim that they can account for the position and shape of this circular dichroism band by assuming that optical activity is induced in an ionized tyrosine residue by the coenzyme. Furthermore, they report that when pyridoxal-P N-oxide, a pyridoxal-P analog which is incapable of accepting a proton at its ring nitrogen, is used to reconstitute the holoenzyme the circular dichroism spectrum is characteristic of an unionized tyrosine residue.

The binding to the pyridine nitrogen is considered by Ivanov and Karpeisky to be responsible for lowering the pkg of the imine nitrogen from a solution value of 10.5 to approximately 8. An additional pkg lowering effect to the observed value of 6.2 is attributed to the presence of a positively charged group X⁺ in the active site. In Figure 19 are shown the possible ionic and tautomeric forms of the pyridoxal-P Schiff's base in solution and under the particular conditions existing in the active site of aspartate aminotransferase.

At the lower end of the range of pH values at which the enzyme is active (pH 6.0-9.5), it is clear that an N-protonated amino acid substrate interacts with the dipolar form of the coenzyme. In a model Schiff's base reaction, however, the reaction rate goes through a maximum as a function of pH, indicating that the most favorable reactants for the nucleophilic addition reaction are a deprotonated amino acid

Figure 19. Pyridoxal-P Schiff's base in solution and enzyme

and a protonated carbonyl group. 23

$$c = oH^+ + RNH_2$$
 $= c = NR + H_2 o$

Ivanov and Karpeisky reconcile this fact with the conditions of the ensyme reaction by proposing a reaction step in which there occurs deprotonation of the amino acid in favor of the imine nitrogen of the coensyme. This step is made possible by neutralization of the positively charged group X^+ by the carboxylic group of the substrate; the effect of this group in lowering the pK of the imine nitrogen is thus eliminated and the value of the pK returns from 6.2 to approximately 8. Under the influence of X^+ the pK of the substrate amino group is lowered from 9.8 to about 7.7. Thus, immediately before the step of nucleophilic addition the most favorable reactants have been prepared.

Figure 20. Reactants for nucleophilic addition 24

Ivanov and Karpeisky argue that electrostatic forces orient the substrate amino acid at the active site in such a way that the lone pair of the substrate amino acid nitrogen is aligned with the p_z orbital of the formyl carbon atom with a distance of no less than the sum of the van der Waals' radii of the two atoms, or 3.5 Å. A sufficient condition for reducing this distance to the length of 1.5 Å necessary for a covalent single bond can be achieved by displacement of the coenzyme molecule. The conformational mobility required for this movement is made possible because the protonation of the imine nitrogen causes a drop in the pK_z of the pyridine nitrogen to between 6.0 and 6.5. The hydrogen bond with the tyrosine residue is disrupted and, once freed of this anchor, the coenzyme can rotate by an angle of about 40° about an axis passing through its methyl and phosphate groups. The rotation is 'locked' into place by formation of the covalent bond between the amino acid nitrogen and the formyl carbon.

At this stage in the reaction, the formyl carbon is bonded tetrahedrally as shown in Figure 21. In the next step, a proton is transferred from the substrate nitrogen to the nitrogen of the ξ-amino group of the lysine residue of the protein and the bond to the latter group is disrupted. Immediately following the breaking of the bond, this group is still able to accept a proton and the authors claim that the proton of the α-carbon is thereby abstracted, with formation of the quinonoid intermediate. This idea is consistent with the fact that aspartate aminotransferase displays a pH independent V in the pH range 6.0-9.5 and may be explained if protonation-deprotonation steps are assisted by internal protein residues so that no protons are released to or taken up from the medium at any stage of the reaction.

Figure 21. Formyl carbon bonded tetrahedrally 24

Metzler et al.⁵ analyze the absorption spectrum of aspartate aminotransferase by fitting individual ionic and tautomeric spectra with lognormal distribution curves. The pyridoxal-P Schiff's bases on the enzyme have peaks shifted bathochromically by about 1100 cm⁻¹ from the positions of the peaks of the model compounds. Metzler et al. suggest the presence of a nearby positive charge or different conformations. Vibrational structure of the absorption bands suggests that the pyridine mitrogen is protonated.

Arrio-Dupont¹⁷ reports the fluorescence spectrum of aspartate aminotransferase. The 360 nm absorbing form displays an emission at 430 nm, while the 430 nm absorbing form emits at 520 nm. On the basis of comparison with the fluorescence properties of model compounds, Arrio-Dupont proposes the structures shown in Figure 22.

$$P \xrightarrow{N \to H^{\pm} Y} P \xrightarrow{$$

Figure 22. Active site of aspartate aminotransferase 17

C. GLYCOGEN PHOSPHORYLASE

In the pH range 5-9, glycogen phosphorylase catalyzes the following reaction:

phosphate + amylose(n + 2) \rightleftharpoons glucose-1-P + amylose(n + 1)

Pyridoxal-P is required for activity and is linked to an enzyme lysine residue, but the biochemical role of the coenzyme is unclear.

In addition to a 280 mm protein absorption, glycogen phosphorylase exhibits a major absorption band at 333 nm and a minor absorption band at 425 nm. ¹⁷ The emission spectrum of glycogen phosphorylase has two bands, one at 335 nm due to the aromatic amino acid residues in the protein and one at 535 nm due to pyridoxal-P. ¹⁷

Pased on the study of pyridoxal-P Schiff's bases in nonaqueous solvents, Arrio-Dupont¹⁹ concludes that the 333 nm absorption is due to an enclimine form of the pyridoxal-P Schiff's base in a hydrophobic environment. Upon excitation of this form, however, fluorescence is found to occur entirely from the ketoenamine form which is reached by proton transfer across the chelate hydrogen bond in the excited state, as shown previously in Figure 12.

Shaltiel and Cortijo²⁶ observe that the 425 nm absorption increases with the addition of urea at neutral pH. Apparently the effect of denaturing the protein is to expose the pyridoxal-P Schiff's base to the more polar aqueous environment that favors the ketoenamine form.

Jones and Cowgill²⁷ suggest that upon excitation at 280 nm energy transfer occurs from the tryptophan residues of the protein to the 335 nm absorbing form of the coenzyme which then emits at 515 nm. As

evidence, they report the observation of a peak in the excitation spectrum of the protein-bound pyridoxal-P at 280 nm that is not present in the excitation of free pyridoxal-P. A problem with this conclusion, however, is the fact that pyridoxal-P Schiff's bases absorbing at about 420 nm generally have a higher energy absorption maximum near 280 nm. Cortijo et al. 28 explore the question of energy transfer more carefully. The quantum yield of the apoenzyme was determined to be $Q_0 = 0.18$ and that of the holoenzyme to be $Q_T = 0.12$. From these values, assuming the difference to be purely a result of energy transfer, the efficiency of energy transfer was calculated:

$$T = (1 - Q_T/Q_0) = 0.33$$

Since this transfer may occur from as many as twelve different tryptophan residues, the authors do not try to interpret this parameter in terms of a distance, but they do suggest that transfer efficiency may be a rather sensitive measure of conformational change.

Shimomura and Fukui²⁹ cite studies that show that pyridoxal-P is buried inside the protein with the 5'-phosphate group near the substrate site. They report a maximum in absorption at 251 nm in addition to the one at 335 nm in the difference spectrum between the holoenzyme and the apoenzyme. These absorptions are characteristic of an enclimine form of the pyridoxal-P Schiff's base.

A micellar experimental model for the pyridoxal-P site of glycogen phosphorylase is proposed by Gani et al.^{7,8} based on their studies of pyridoxal-P bound to mixed micelles of long chain alkylamines. The absorption spectrum of a mixed micelle of hexadecyltrimethylammonium bromide and n-dodecylamine to which pyridoxal-P binds stoichiometrically

to the latter component displays absorption maxima at 333 nm and 250 nm. The fluorescence spectrum displays a maximum at 550 nm upon excitation at 335 or 415 nm. Four possible structures absorbing at 325-335 nm are shown in Figure 23. The authors favor structure G in which the pyridoxal-P is embedded in a hydrophobic microenvironment but in which there is an abrupt drop in hydrophobicity in the vicinity of the coenzyme that allows hydrophilic substances to approach closely.

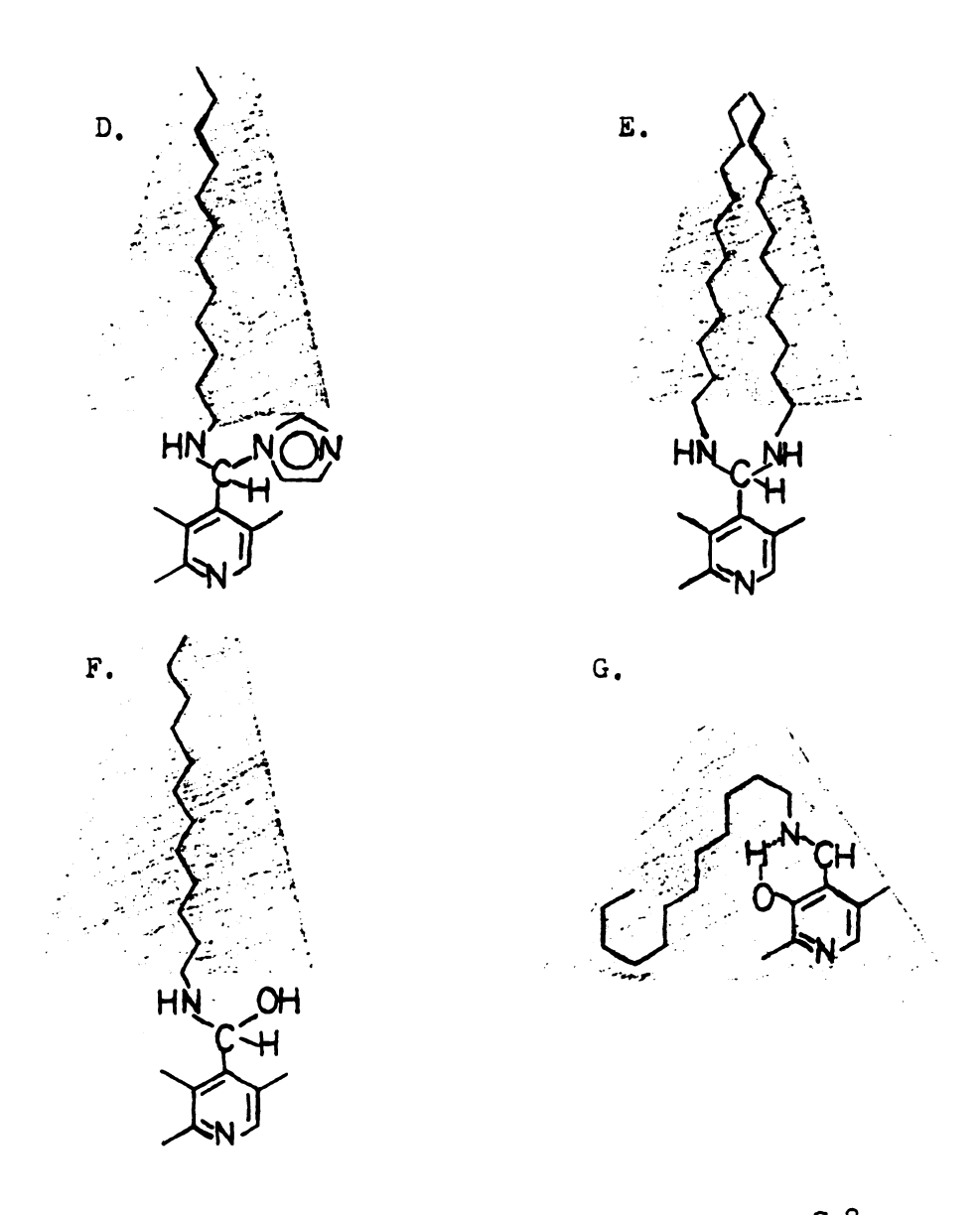


Figure 23. Pyridoxal-P Schiff's base micelle 7,8

D. TRYPTOPHANASE

A recent review by Snell²⁹ details the properties of tryptophanase, which catalyzes the \angle , β -elimination reaction

as well as several related reactions. Tryptophanase is a tetrameric protein with four identical subunits each of molecular weight 55,000, which binds one pyridoxal-P molecule per subunit.

A pH titration of the enzyme from \underline{E} , $\underline{\operatorname{coli}}$ in imidazole-HCl plus 0.1 M KCl and 0.1 M potassium carbonate buffers shows two pH dependent absorption maxima at 337 and 420 nm with an apparent pK_a of 7.4. In the presence of sodium or imidazole alone, only the 420 nm band is observed. These absorption spectra are shown in Figures 24 and 25.

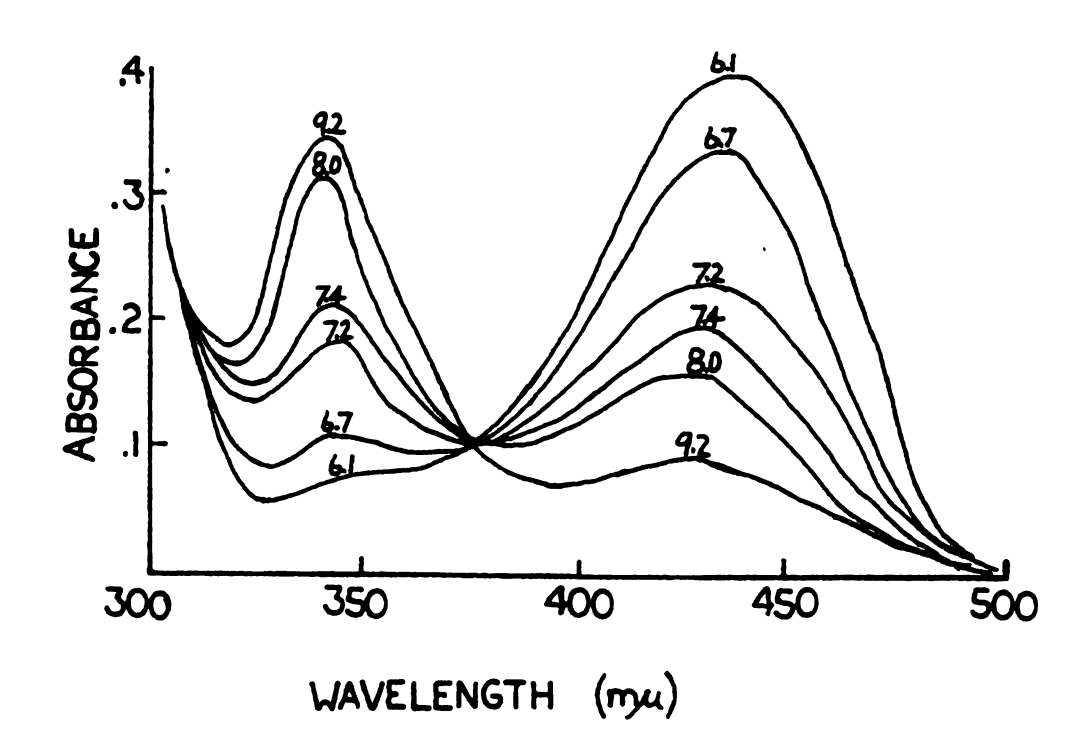


Figure 24. Absorption spectra of tryptophanase as a function of pH29

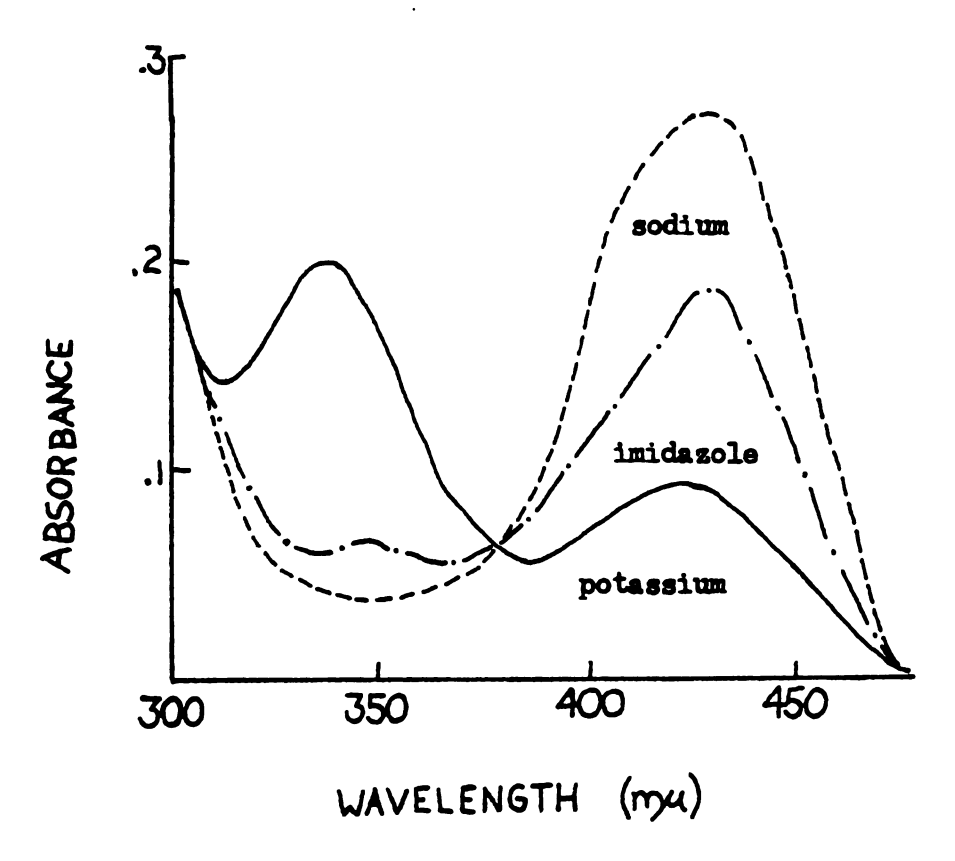


Figure 25. Absorption spectra of tryptophanase as a function of cation 29

In tryptophanase, pyridoxal-P is present in an azomethine linkage with the &-amino group of a lysine residue. The mechanism of action of tryptophanase is given by Snell as shown in Figure 26.²⁹ Briefly, the substrate amino acid forms a Schiff's base with the coenzyme pyridoxal-P and a proton is labilized at the &-carbon. The indole group leaves, followed by the separation of an aminoacrylate which then is degraded to the products pyruvate and ammonia.

Tryptophanase exhibits a requirement for monovalent cations. In his discussion of enzymes activated by monovalent cations, Suelter³¹ points out that many enzymes are activated by potassium, rubidium, and ammonium but not by lithium or sodium. He suggests that monovalent cations may participate in the enzyme-substrate complex or assist in the control of enzyme conformation, or both. A potential keto-enol tautomer might be

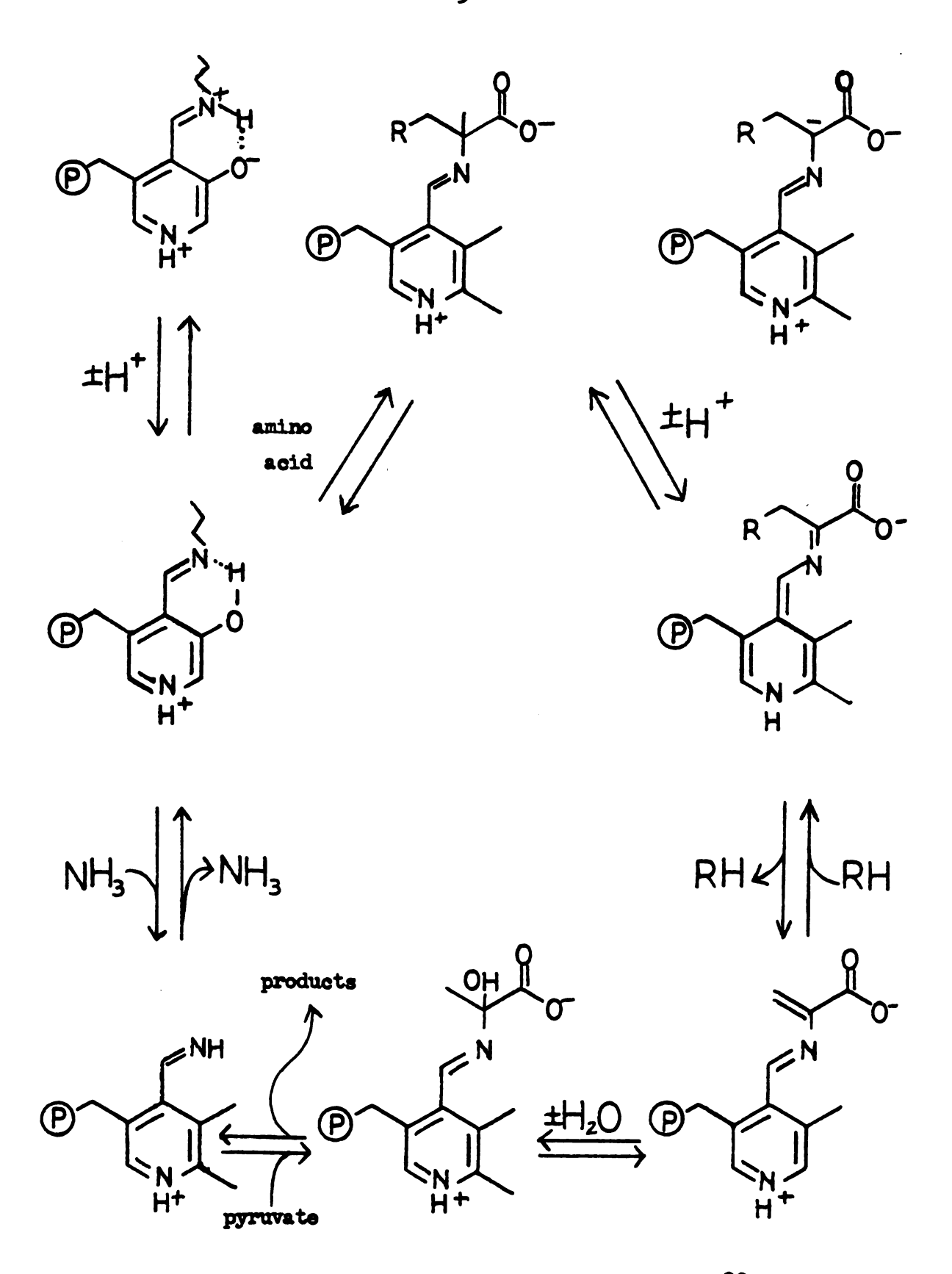


Figure 26. Mechanism of action of tryptophanase²⁹

involved in binding the monovalent cations.

Snell²⁹ indicates that a large conformational change occurs in the interconversion of holo- and apotryptophanase. The fact that sedimentation rate increased much more in the presence of potassium than in the presence of sodium indicates that potassium promotes a 'tightening' of the enzyme structure or a major change in shape, or both.

The role of monovalent cations in promoting tight coenzyme binding to the protein is compared to cation activity as a cofactor by Toraya et al. 32 Holoenzyme solutions containing 0.1 M of the cation as its chloride were resolved of the coenzyme pyridoxal-P by gel filtration. Ability to hold the pyridoxal-P and cofactor activities were high for potassium, rubidium, and ammonium and low for sodium, lithium, and cesium. The affinity of the sodium enzyme for pyridoxal-P was shown to be much lower ($K_D > 31\mu M$) than that of the potassium enzyme ($K_D = 1.8\mu M$).

A possible defect in the preceding study is the fact that the investigators may have failed to use saturating concentrations of the monovalent cations. The values reported by Suelter and Snell³³ for the activating constants for the various cations at 25° C obtained in 0.6 mM S-orthonitrophenyloysteins are given in Table 1. These authors assert that each cation activates and that the K_{m} for SOPC is not significantly affected by cation with the exception of sodium, whereas V_{max} changes and can be taken as a measure of cofactor activity. Failure to observe activity in previous work may therefore be a result of too little cation in the assay mixture. Presumably this fact would affect the K_{D} values reported by Toraya et al. as well.

Suelter and Snell³³ discuss the interaction of the cation with the ensyme in terms of the difference in free energy of hydration of the

cation and the free energy of interaction of the naked cation with its binding site on the enzyme surface. These differences are in the order potassium \rangle rubidium \rangle cesium \rangle sodium \rangle lithium. Further, they point out that cations between 1.3 % and 1.5 % in ionic radius are the best activators.

Table 1. Activating constants for monovalent cations 33

Cation	K _D (mM)
Lithium	54 + 11.6
Sodium	40 + 0.06
Potassium	1.44 + 0.06
Thallium(I)	0.95 + 0.1
Ammonium	0.23 + 0.01
Rubidium	3.5 + 0.3
Cesium	14.6 + 2.6

The complex between holoenzyme and the dead-end inhibitor L-ethiomine in the presence of activating cation develops a strong 508 nm absorption band, whereas there is only a small spectral change in the absence of cation. Circular dichroism results indicate that L-ethionine is
bound to the enzyme in either case. Thus, Suelter and Shell are able to
conclude that monovalent cations are necessary for converting the ensyme-L-ethionine complex to the 508 nm absorbing form in which the proton
on the ck-carbon of L-ethionine has been labilized.

Hogberg-Raibaud et al. Hogberg-Raibaud et al.

activation of the enzyme by potassium and ammonium in the presence of saturating concentrations of pyridoxal-P and found sigmoidal curves with Hill coefficient of 2.7 for potassium and 1.5 for ammonium. A concentration of 0.1 M potassium was adequate to saturate the enzyme; at 0.4 M potassium, about 20% inactivation was observed. Högberg-Raibaud et al. favor an interpretation of their results as a cooperative interaction between protomers in which the binding of potassium to one protomer leads to an increased affinity by the other protomers.

At saturating potassium concentrations, the binding of pyridoxal-P is followed by the appearance of activity in the apoenzyme. In phosphate buffer, there are two kinetically distinct steps with rate constants 0.49 min⁻¹ and 0.095 min⁻¹. A model of pre-existing equilibrium between two apoenzyme conformations, only one of which binds pyridoxal-P, is discarded on the basis of a linear Scatchard plot in favor of an anti-cooperative model. A conformational change upon binding might be used to account for the slow dissociation kinetics observed for the holoenzyme. Because phosphate ion is known to inhibit reconstitution of holo-aspartate aminotransferase, a Tricine-KOH buffer system was also used with results similar to those for phosphate buffer.

Finally, Hogberg-Raibaud et al. measure the K_D for binding pyridoxal-P to apotryptophanase in the presence of potassium to be 0.4 μ M. Earlier reports of K_D are criticized for not allowing sufficient time for complete reconstitution of the holoenzyme.

Fenske and DeMoss³⁵ report the fluorescence spectrum of tryptophanase from <u>B</u>. <u>alvei</u>. Upon excitation at 280 nm, there is an emission at 350 nm for the apoenzyme and emissions at 350 and 510 nm for the holoenzyme. Resonance energy transfer from the tryptophan residues of the

protein to the pyridoxal-P is suggested as an explanation for the 510 nm emission since free pyridoxal-P does not absorb at 280 nm. However, it should be remembered that the enzyme bound Schiff's base may well absorb at 280 nm.

Isom and DeMoss³⁶ report hyperbolic kinetics from a spectrophotometric study of the binding of pyridoxal-P to the apoenzyme, with a K_D value of 1.6 M. A similar value was obtained by studying the quenching of apoenzyme fluorescence upon binding of pyridoxal-P. An average maximum of 44% of apoenzyme fluorescence could be quenched.

The effect of pH on the fluorescence of holotryptophanase is also reported by Isom and DeMoss. ³⁶ A form excited at 340 nm and emitting at 400 nm grows from pH 7.1 to pH 9.0, followed by a decrease at pH 9.3; a form excited at 420 nm and emitting at 510 nm grows from pH 9.3 to pH 7.1. However, since these investigators were working at 0.75 mg/ml, or 14 \mu M in bound pyridoxal-P (MW = 52,000 per pyridoxal-P binding site), and the 100 \mu M free pyridoxal-P in solution has forms absorbing at 330 and 390 nm and emitting near 400 and 500 nm, respectively, it is difficult to have much confidence that they are seeing coenzyme fluorescence alone.

A computer analysis of the changes in the absorption spectrum of native holotryptophanase with pH gives absorption spectra of the protonated and deprotonated forms. 36 In 0.05 M potassium phosphate buffer containing $100\,\mu$ M pyridoxal-P the authors report a pK of 7.89 + 0.019. However, the concentration of potassium is not high enough to saturate the enzyme if Suelter and Snell's 33 values for the E. coli enzyme apply. Furthermore, Isom and DeMoss do not mention using sulfhydryl compounds to protect their enzyme as is necessary with tryptophanase from E. coli.

In a companion paper, Isom and DeMoss³⁷ report that the K_D value for pyridoxal-P binding to apotryptophanase in the presence of sodium is tenfold higher than in the presence of potassium. They also studied the binding of ANS to the apoenzyme; ANS fluorescence was enhanced and the emission maximum shifted as is characteristic of ANS in a hydrophobic environment. Since they were also able to show that ANS is a competitive inhibitor of coenzyme binding, they were able to conclude that a hydrophobic region exists at the active site of tryptophanase.

CHAPTER 3

AN HYPOTHESIS REGARDING THE ROLE OF MONOVALENT CATIONS IN TRYPTOPHANASE

There are at least two forms of holotryptophanase including a form that absorbs at 420 nm and a form that absorbs at 337 nm; the latter form is observed only in the presence of activating monovalent cations and at sufficiently high pH values. Morino and Smell 38 identify the 337 nm absorbing form as a nonhydrogen bonded azomethine, as shown in Figure 27. They do not account for the fact that the same structure in the ensyme aspartate aminotransferase absorbs at the longer wavelength of 360 nm. Snell and Dimari 39 point out that there are a variety of ionic and tautomeric forms possible including those differing by a proton on the pyridine mitrogen and they therefore conclude that the exact structure is not certain. Snell²⁹ draws another structure for the 337 nm form, also shown in Figure 27, and he suggests that this hydrogen bonded structure could be favored in the hydrophobic environment of the enzyme active site as in the case of glycogen phosphorylase where this structure is present and absorbs at 333 nm. However, unlike phosphorylase, holotryptophanase can be reduced and inactivated by sodium borohydride. Thus, no structure for the 337 nm form is consistent with all of the available information.

Since the first steps in the mechanism of α , β -elimination are

Figure 27. Possible 337 nm forms

apparently identical to those of transamination, it would be reasonable for coenzyme attachment to be the same in both these classes of enzymes. Ivanov and Karpeisky 24 identify a dipolar form of the coenzyme in aspartate aminotransferase that is stabilized by the presence of a positive charge from the enzyme. By analogy, the role of the monovalent cation required by tryptophanase can be explained. Specificity for certain cations would be a result of the need to fit into a protein 'pocket' that holds the cation in place near the phenolic group. In particular, the cation would have the function of increasing the pK_a of the pyridine nitrogen and decreasing the pK_a of the imine nitrogen. Structures of the coenzyme in the active sites of aspartate aminotransferase and tryptophanase according to this hypothesis are shown in Figure 28.

Provided this hypothesis is correct, why does this form absorb at 337 mm in tryptophanase instead of at 360 mm as in aspartate aminotransferase? Referring to Figure 2, one can expect a variation in spectral wavelength from 367 mm (Structure II) to 322 mm (Structure I) as a

Figure 28. Analogous coenzyme forms

positive charge approaches the 0 group. The absorption maximum is at longer wavelengths the more the electron on the oxygen is delocalized into the ring, which in general depends on the state of protonation of the phenolic oxygen and the imine nitrogen in the model compounds. In the ensymes under discussion, one can think of other positive charges playing a role similar to that of the proton. From the spectral maxima it appears that in tryptophanase the monovalent cation is more effective in localizing the electron on the phenolic oxygen than is the positively charged residue in aspartate aminotransferase, but less so than a proton. Another effect that can give rise to spectral shifts is for the protein to hold the pyridoxal-P Schiff's base in different conformations about the bond between the pyridine ring and the azomethine carbon atom.

Since protonation at the pyridine nitrogen has little effect on the absorption maximum of B_6 enclimines (see Figure 4), there is another form that absorbs near 337 nm differing from the one discussed above by a proton. The 420 nm absorber is similar to Structure III, Figure 2,

represented in its major resonance form in Figure 3. Again, there are two possible forms absorbing near 420 mm differing in state of protonation of the pyridine nitrogen. Protonation of the pyridine nitrogen is promoted by the presence of activating menovalent cations.

Another implication of Ivanov and Karpeisky's model of aspartate aminotransferase is the necessity for rotation of the coenzyme in going from a form in which the pyridine nitrogen is protonated to one in which it is depretonated (hydrogen bond to protein tyrosine residue disrupted). In tryptophanase, the presence of activating monovalent cations would affect the position of the equilibrium between these forms. Going one step further, it is easy to think of this proton transfer-coenzyme rotation as being coupled to a change in protein conformation. If the conformational change is slow, there is a possibility of observing slow spectral interconversions after an abrupt change in pH or monovalent cation.

An interesting point that may be important in interpreting the luminescence properties and action of light on the enzyme has been raised by Ivanov and Karpeisky. They discuss the possibility of an excited state proton transfer reaction from a protein residue to the imine nitrogen in which the excited state derived from the 360 nm absorber is converted into the excited state derived from the 430 nm absorber; these emit at 430 nm and 505 nm, respectively. If this reaction is carried out to any extent within the lifetime of the excited state, excitation at 360 nm might result in an emission at 505 nm. Although this is not the case in aspartate aminotransferase, another enzyme active site might have a greater availability of protons and thus enable one to observe the phenomenon of intermolecular excited state proton transfer.

Intramolecular excited state proton transfer has been suggested as an explanation for the long wavelength emission of glycogen phosphorylase.²¹

CHAPTER 4

RESULTS AND DISCUSSION

A. ABSORPTION AND EMISSION STUDIES

Several studies of the absorption spectra of tryptophanase under various conditions were reported (Chapter II). In the present work, a study of the absorption characteristics of the enzyme was undertaken in order to reproduce and extend previous results as a basis for the study of the fluorescence properties of tryptophanase and the interpretation of rapid scanning stopped flow kinetics data.

Absorption spectrum of apotryptophanase. The absorption spectrum of apotryptophanase in 25 mM K-EPPS, pH 8.0, was measured against a blank of the same buffer and the results are shown in Figure 29 (for details of buffer preparation, see Materials and Methods). The peak at 278 mm can be explained by the well known absorption characteristics of the aromatic amino acid residues of the protein.

Difference spectrum between bound and free pyridoxal-P. The previous enzyme sample was diluted 1:10 with K-EPPS containing 100 \(\mu\) M pyridoxal-P and blanked against the same proportions of K-EPPS and K-EPPS containing 100 \(\mu\) M pyridoxal-P. The absorption spectrum was measured after 50 min. at 22°C and this spectrum is also shown in Figure 29 corrected for the dilution. After subtraction of the apoenzyme absorption, the difference spectrum between bound and free pyridoxal-P has maxima at

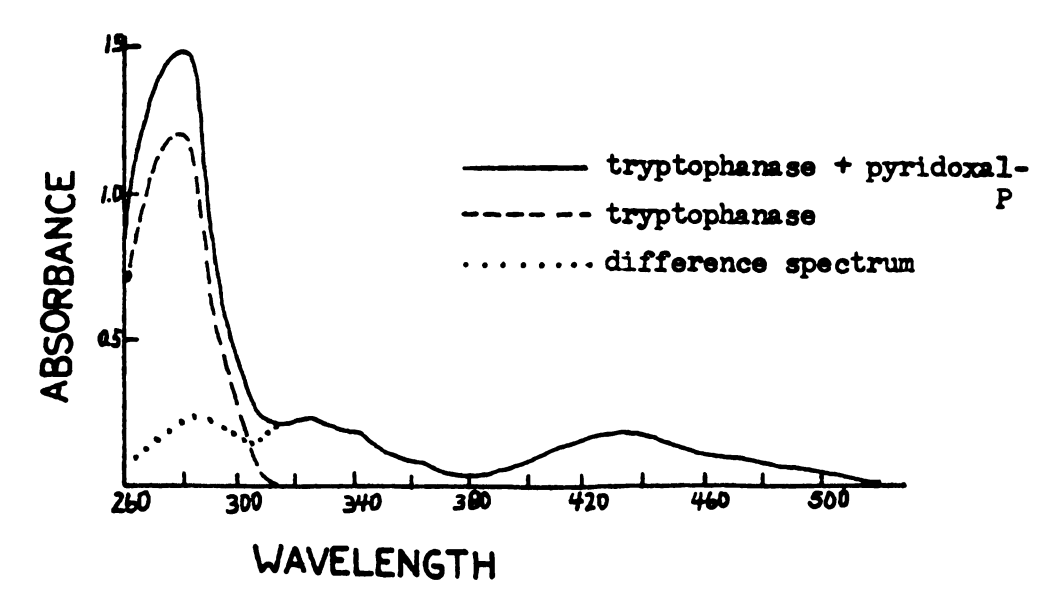


Figure 29. Absorption and difference absorption spectra

430, 380, 360, 337, and 325 mm. This difference spectrum represents the difference in absorption between the 337 and 420 mm forms of bound pyridoxal-P and the numerous forms absorbing in the visible region of the spectrum for free pyridoxal-P. The 430 nm peak represents a change in absorption as a result of the reaction shown in Figure 30, which can also account for the peaks at 325, 360, and 380 nm. The peak at 337 nm is due to the fact that bound pyridoxal-P also has a 337 nm form.

$$\mathbb{P} \xrightarrow{\mathbb{N}} \mathbb{P} \xrightarrow{\mathbb{N}} \mathbb{N}$$

Figure 30. Pyridoxal-P binding reaction

The difference in the heights of the 280 mm peaks in the spectra of the apoenzyme and apoenzyme to which pyridoxal-P has been added can be attributed to the absorption of the bound pyridoxal-P at 280 mm. Model studies indicate that the 420 mm form of the pyridoxal-P Schiff's base absorbs strongly at this wavelength, whereas free pyridoxal-P does not.

Fluorescence spectrum of apotryptophanase. The fluorescence spectrum of apotryptophanase in K-EPPS excited at 280 nm was obtained, as shown in Figure 31. There is one emission maximum occurring at about 360 nm, corresponding to the emission of the tryptophan residues in the protein.

Absorption spectrum of holotryptophanase in the presence of tetrame-thylammonium. In an initial study of holotryptophanase absorption, an attempt was made to reproduce the results of Suelter and Snell. 33 Holotryptophanase in activation buffer was passed over Sephadex G-25 fine (1x22 cm), eluted with TMA-EPPS buffer, and collected in 0.5 ml fractions; the fractions containing the highest concentrations of tryptophanase were pooled. In the absorption spectrum of the sample, the overall intensity due to bound pyridoxal-P is low relative to the height of the protein peak as compared to the spectra of Suelter and Snell. This appears to be due to a resolution of pyridoxal-P from the holoenzyme in the process of preparing the enzyme on Sephadex gels. This phenomenon is discussed in the work of Toraya et al. 32 Upon addition of 0.15 M KCl and 10 mM L-ethionine, a 508 mm peak developed as reported by Suelter and Snell. However, the intensity of this peak relative to the enzyme peak also was much diminished.

Since the pyridoxal-P - apoenzyme complex is quite labile in the

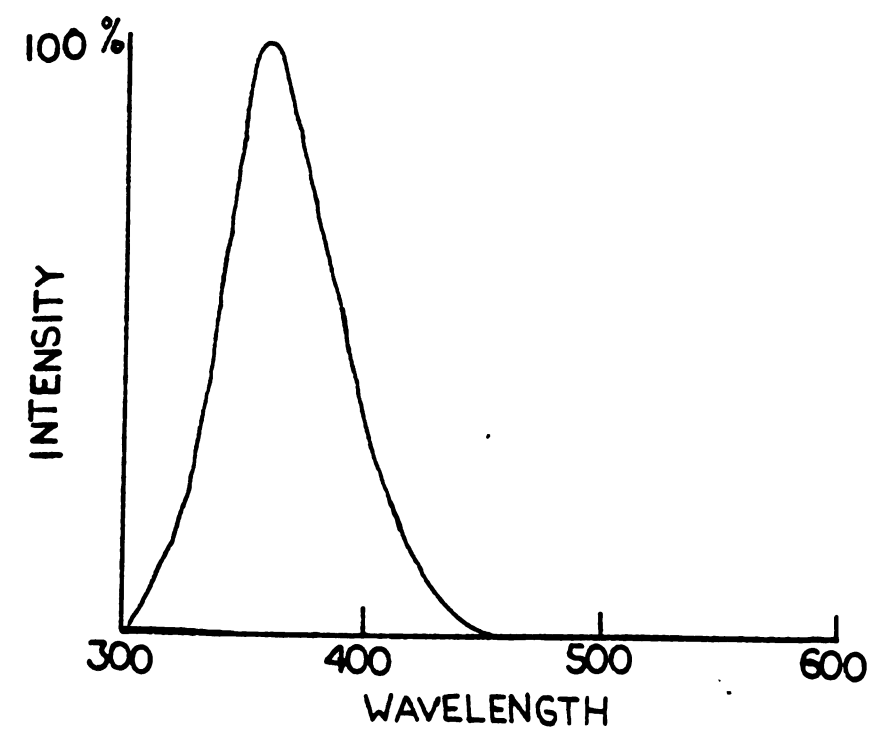


Figure 31. Fluorescence spectrum of apotryptophanase

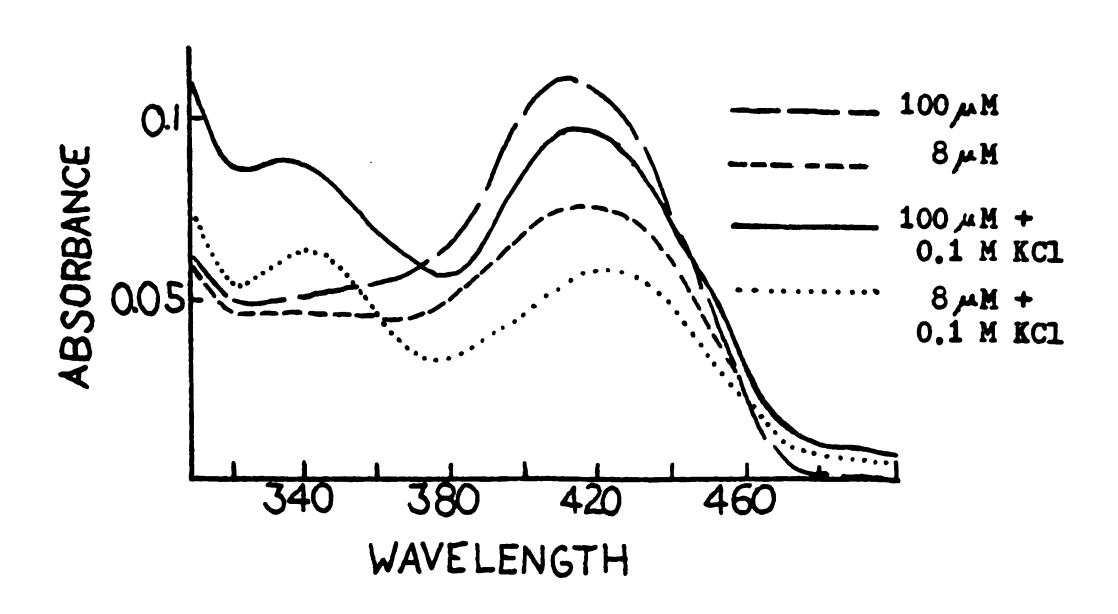


Figure 32. Absorption spectra of tryptophanase in TMA

absence of monovalent cations, it is necessary to incorporate adequate amounts of pyridoxal-P in samples in order to maintain a high degree of binding. As an estimate, one might assume a K_D of 4 µM based on the value given by Isom and DeMoss³⁷ for tryptophanase in the presence of sodium, a cation which does not activate except at very high concentrations. Consider a simple mass action model in which the free pyridoxal-P concentration is fixed by means of equilibrium dialysis and in which E represents enzyme pyridoxal-P binding sites.

Using the conservation equation

one can derive the equation

Fractional saturation =
$$\frac{E-pyridoxal-P}{E_{total}} = \left(1 + \frac{K_D}{pyridoxal-P}\right)^{-1}$$

Notice that this result is independent of enzyme concentration. By substitution into the last equation, one can calculate the pyridoxal-P concentration necessary for 95 % saturation to be 76 μ M. This value is to be compared to a concentration of 18 μ M in pyridoxal-P binding sites for a 1 mg/ml tryptophanase solution.

Suelter and Snell³³ dialyzed their tryptophanese sample against TMA-EPPS containing only 8 µM pyridoxal-P. Based on the previous discussion,

it would appear that their enzyme was not completely saturated with pyridoxal-P. In Figure 32 are shown spectra of tryptophanase in which 8μH and 100μH concentrations of pyridoxal-P are fixed by dialysis; in the former case, the enzyme is only somewhat more than half saturated. Absorption spectrum of holotryptophanase in the presence of phosphate. A comparison of the absorption spectrum of tryptophanase in the presence of potassium given in the preceding section with the spectrum of tryptophanase in the presence of potassium in Figure 25 shows a diminished 337 mm/ 420 mm ratio in the former case. Therefore it was decided to study the absorption spectra of tryptophanase in various buffer systems. In Figure 33 are shown the absorption spectra of tryptophanase in potassium phosphate, TMA phosphate, and TMA phosphate including potassium chloride. As compared to the presence of phosphate ion, the presence of tetramethylammonium ion inhibits the formation of the 337 nm band. This statement is consistent with the observation of Suelter and Snell³³ that tetramethylammonium ion inhibits the tryptophanase reaction.

Absorption spectrum of the holotryptophanase - L-ethionine complex.

10 mM L-ethionine was added to the potassium phosphate sample and the reference solution and the absorption spectrum recorder. The spectrum is shown in Figure 34 and may represent the correct enzyme - L-ethionine complex absorbance relative to the absorbance of the aromatic amino acid residues since the enzyme is completely saturated with pyridoxal-P. The L-ethionine - holoensyme complex in the presence of activating monovalent cations is able to eliminate the proton attached to the &-carbon to give rise to a quinonoid form. The long system of conjugation resembles that encountered in merocyanine dyes, whose spectra are also

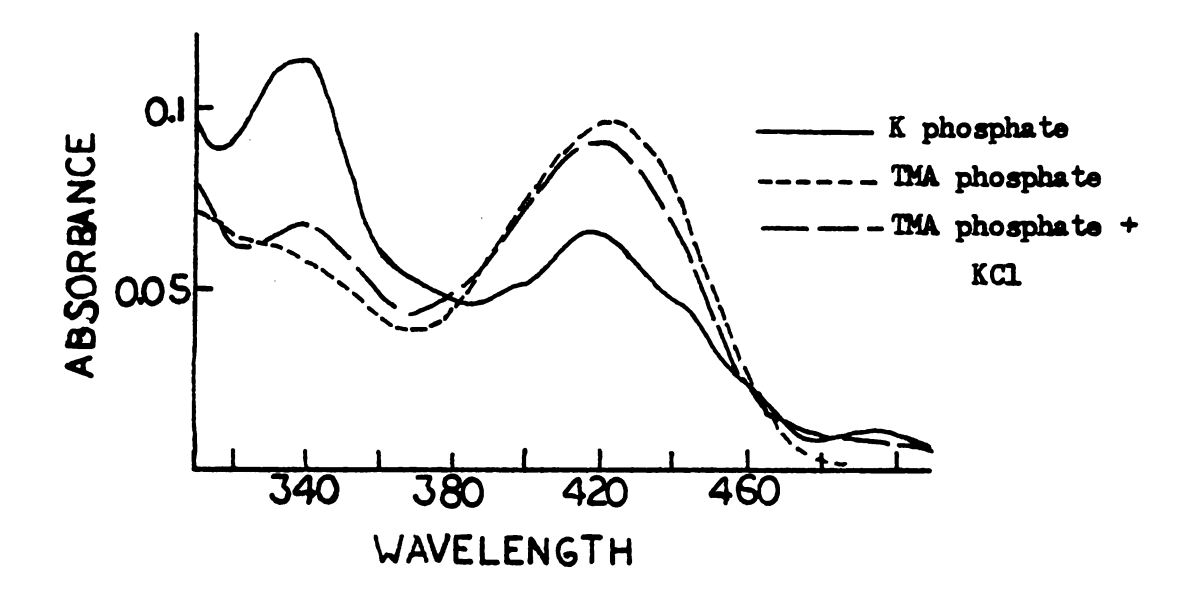


Figure 33. Tryptophanase absorption spectra

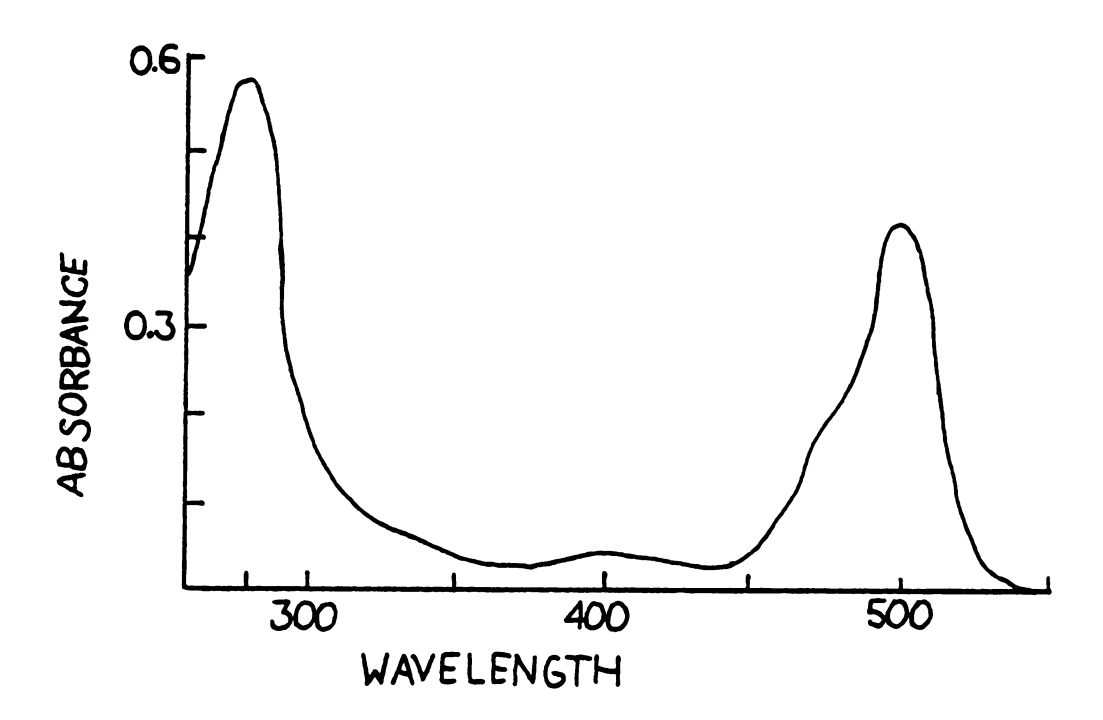


Figure 34. Absorption spectrum of holotryptophanase-L-ethionine

quite similar. 41 They display a definite vibrational structure with a high frequency shoulder and some less pronounced structure at still higher frequencies. The separation of the vibrational peaks, 1000 to 1100 cm⁻¹, corresponds to the frequenct of a C-C stretch.

Fluorescence spectrum of holotryptophanase. In Figure 35 is shown the fluorescence spectrum of tryptophanase in potassium phosphate buffer containing 10 µ M pyridoxal-P, excited at 280 nm. The free pyridoxal-P emits very little when excited at 280 nm so there is little contribution to this spectrum from free pyridoxal-P. The main features of the holotryptophanase spectrum are a 350 nm peak, presumably corresponding to the emission of the tryptophan residues of the protein, a shoulder at about 400 nm, and another emission at 510 nm.

Fluorescence spectrum of the holotryptophanase - L-ethionine complex.

A totally new result is the fluorescence of the holoenzyme -

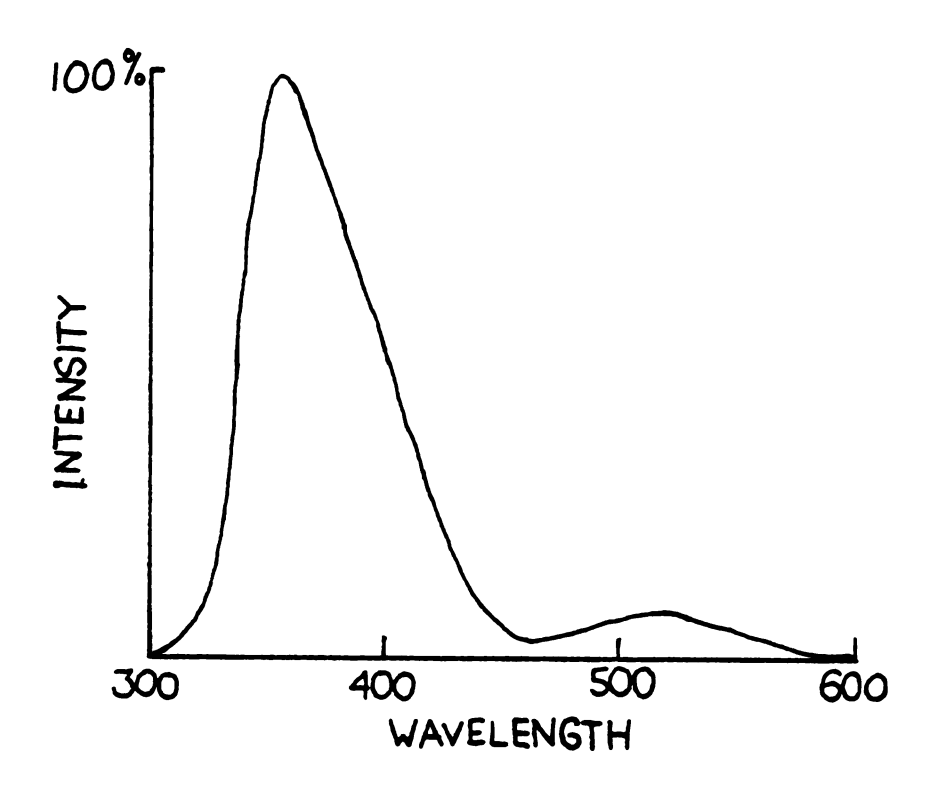


Figure 35. Fluorescence spectrum of holotryptophanase

L-ethionine complex when excited at its maximum absorption wavelength of 508 nm. The fluorescence spectrum is a mirror image of the absorption, with emission maximum at 525 nm.

Absorption spectra of holotryptophanase in the presence of a series of monovalent cations. Concentrations of monovalent cations as their chloride salts were chosen to be at least 10 K_D³³ and, for further convenience in comparing experimental results, buffer and cation concentrations were chosen to agree with a study of pK_a values for the conversion of the 337 form to the 420 nm form. 42 Tryptophanase was prepared in TMA-EPPS, pH 8.0, containing 100 MM pyridoxal-P; the concentrations of the cations are given in Table 2. Results are shown in Figures 36 and 37. Another set of such spectra were obtained for tryptophanase in TMA-CHES, pH 9.0, containing 100 MM pyridoxal-P and the cation concentrations given in Table 2. Solutions containing sodium, lithium, and

Table 2. Concentrations of cations

Salt	Concentration(M)
RbC1	0.5
CsCl.	0,5
NH ₄ Cl	0.025
na	0.6
KCI.	0.1
Na.Cl.	1.0

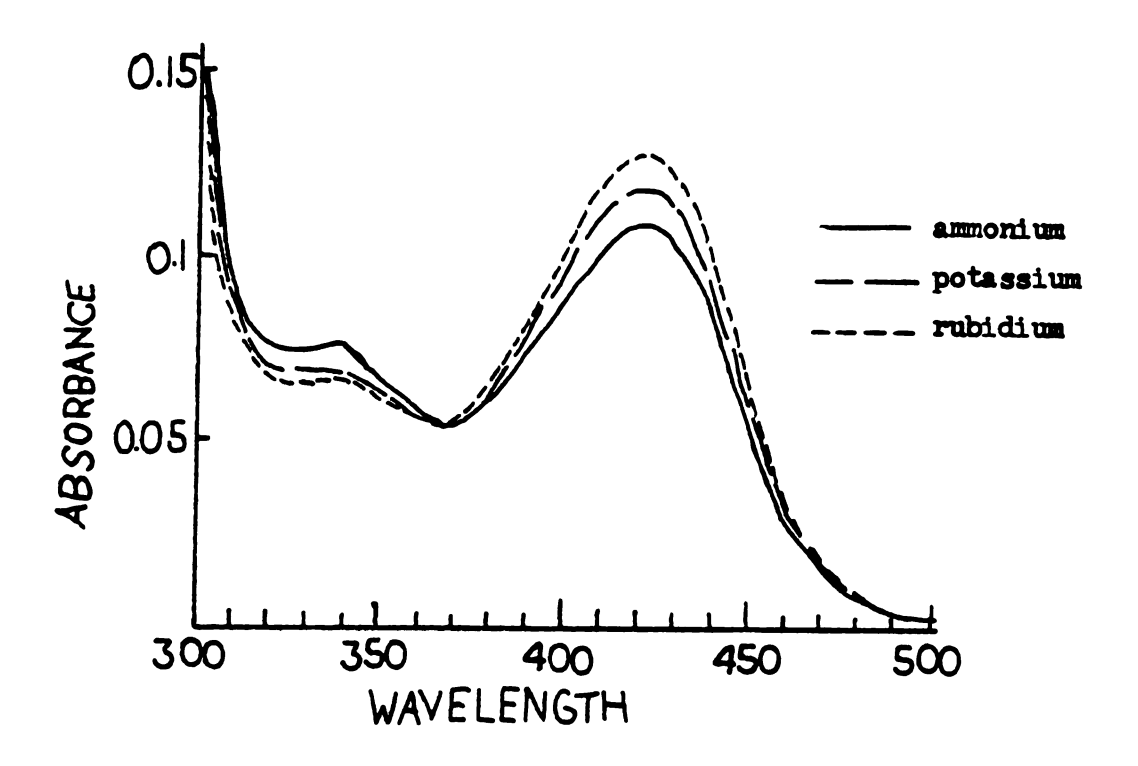


Figure 36. Absorption spectra in ammonium, potassium, rubidium

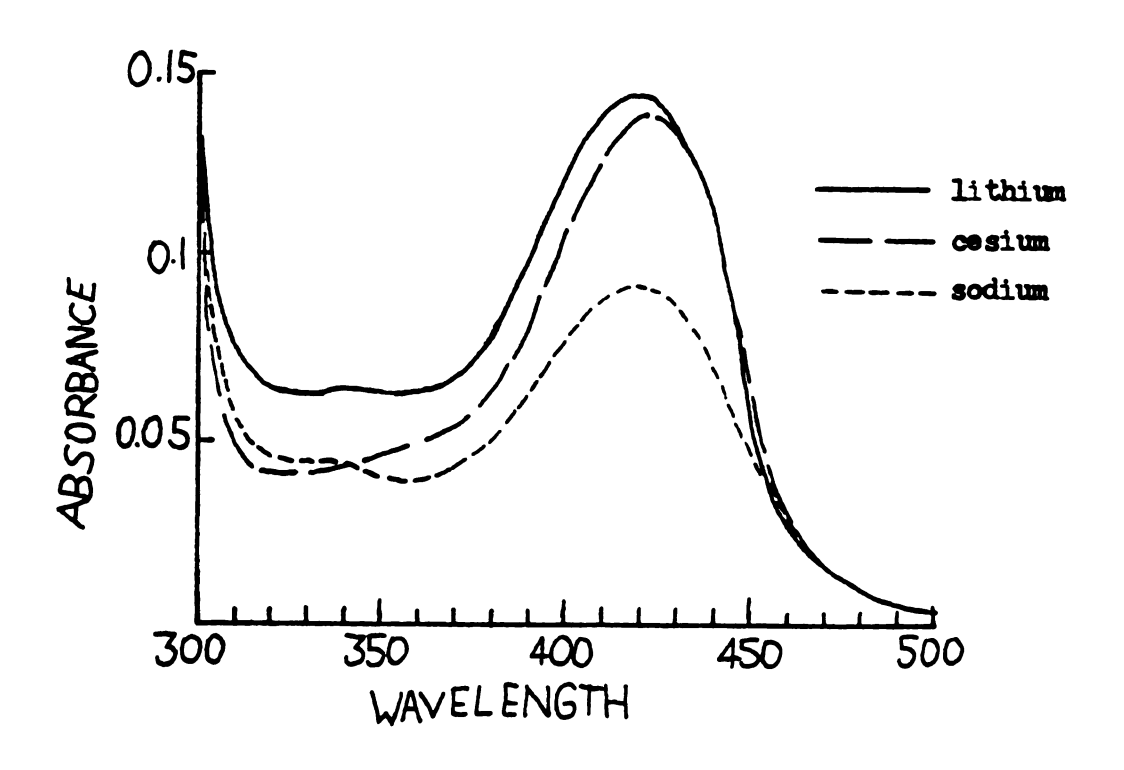


Figure 37. Absorption spectra in sodium, lithium, cesium

cesium lost enzyme activity during overnight dialysis. The absorption spectra of holotryptophanase in the presence of ammonium, potassium, and rubidium at the two pH values are shown in Figures 38, 39, and 40, respectively.

Certain features of these spectra are immediately apparent. Lithium, cesium, and sodium, the cations shown by Suelter and Snell³³ to have only a weak effect in activating the enzyme, exhibit a low ratio of the 337 nm band to the 420 nm band. Cations which activate well, ammonium, potassium, and rubidium, have an enhanced 337 nm absorption and an increased 337/420 nm ratio; the long wavelength peak in the presence of ammonium is red shifted by about 3 nm. In the case of sodium, overall intensity indicates that the enzyme may not be fully saturated

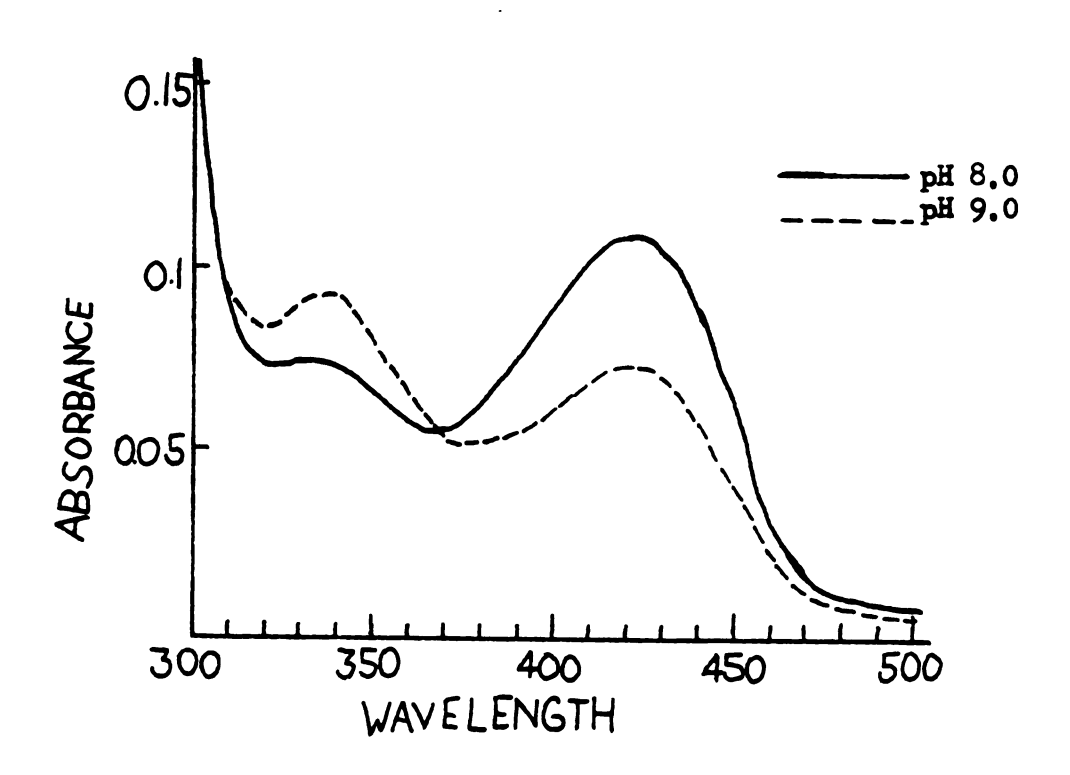


Figure 38. Absorption spectra in ammonium

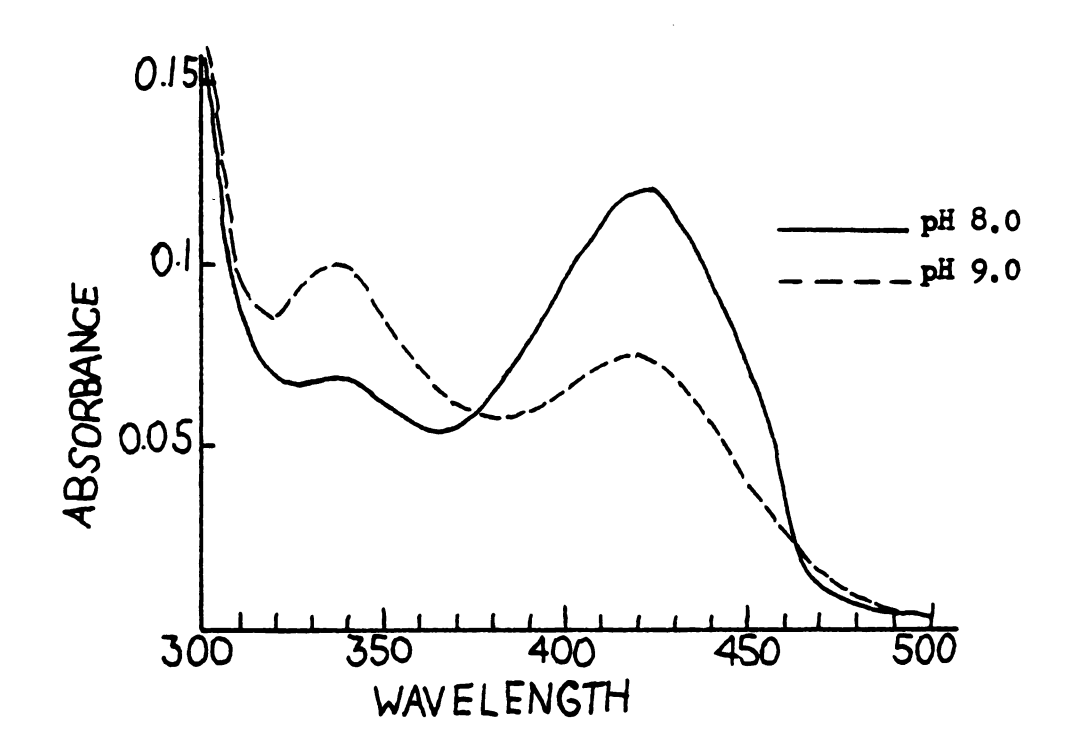


Figure 39. Absorption spectra in potassium

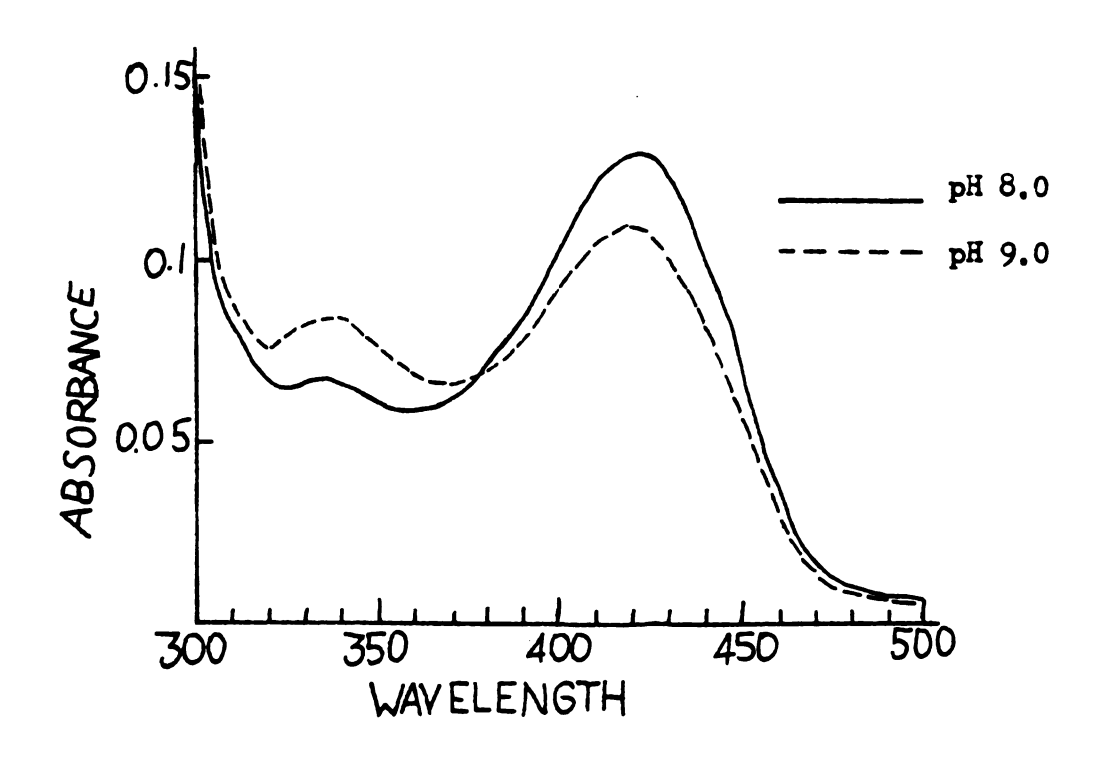


Figure 40. Absorption spectra in rubidium

with pyridoxal-P. The lithium spectrum is also anomalous in that the overall intensity appears to be higher than for the other cations and the long wavelength band is blue shifted by about 3 nm.

In going to pH 9.0, the better activating cations were able to preserve enzyme activity through the period of dialysis. The pH 9.0 spectra display increased 337 nm bands and enhanced 337/420 nm ratios. The large increase in the case of potassium indicates that the pH 8 to pH 9 region is in a steep part of the titration curve, or near the pkg. This observation agrees with the pK value of about 8.5 measured in this buffer. 42 Fluorescence spectra of holotryptophanase in the presence of a series of monovalent cations. Fluorescence spectra were obtained of tryptophanase in TMA-EPPS, pH 8.0, containing 100 µN pyridoxal-P and the concentrations of salts given in Table 2. A typical fluorescence spectrum of the buffer alone excited at 280 nm is shown in Figure 41. The buffer showed large emissions when excited at 340 nm or 420 nm due to the contribution of free pyridoxal-P. In Figures 42, 43, 44, 45, 46, and 47 are shown the fluorescence spectra obtained for tryptophanase in the presence of the various cations, excited at 280 nm. In Figure 48 is shown the fluorescence spectrum of tryptophanase in TMA-CHES, pH 9.0, containing 100 M pyridoxal-P ans potassium as given in Table 2 along with the pH 8.0 spectrum. These spectra are drawn to the same scale as Figure 31 in which the appearage fluorescence intensity is normalized to 100%.

The most striking feature of the fluorescence spectrum of holotryp-tophanase excited at 280 nm is the existence of three emissions. A 350 nm emission is due to the aromatic amino acid residues of the protein and is also present in apotryptophanase. Emissions at 400 nm and 510 nm originate from the 337 and 420 nm forms of bound pyridoxal-P,

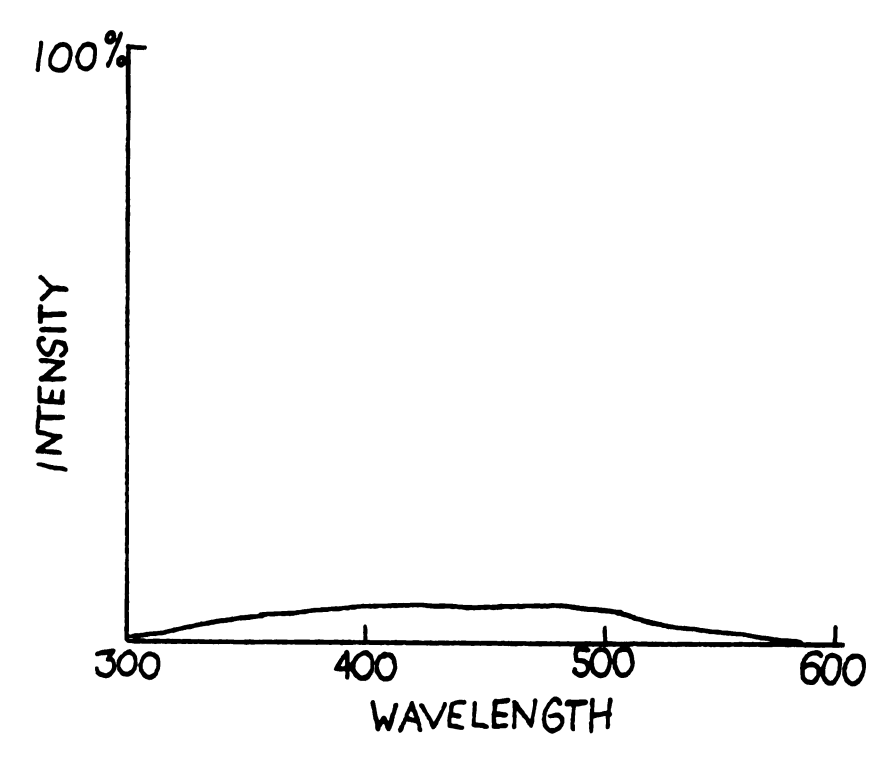


Figure 41. Fluorescence spectrum of buffer

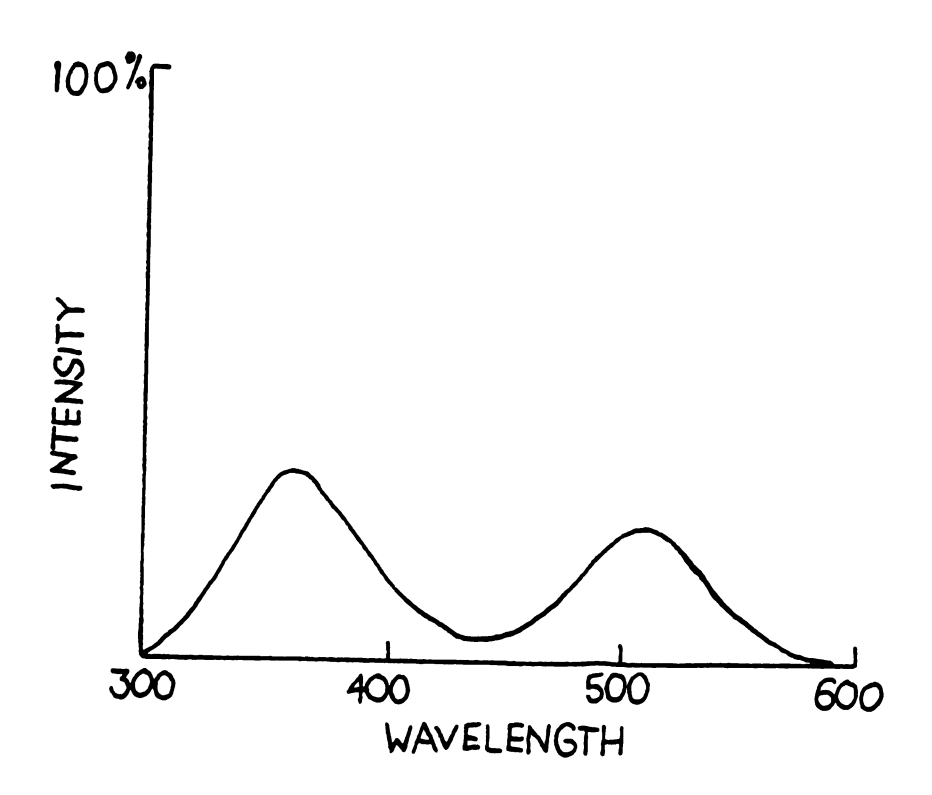


Figure 42. Fluorescence spectrum of tryptophanase in ammonium

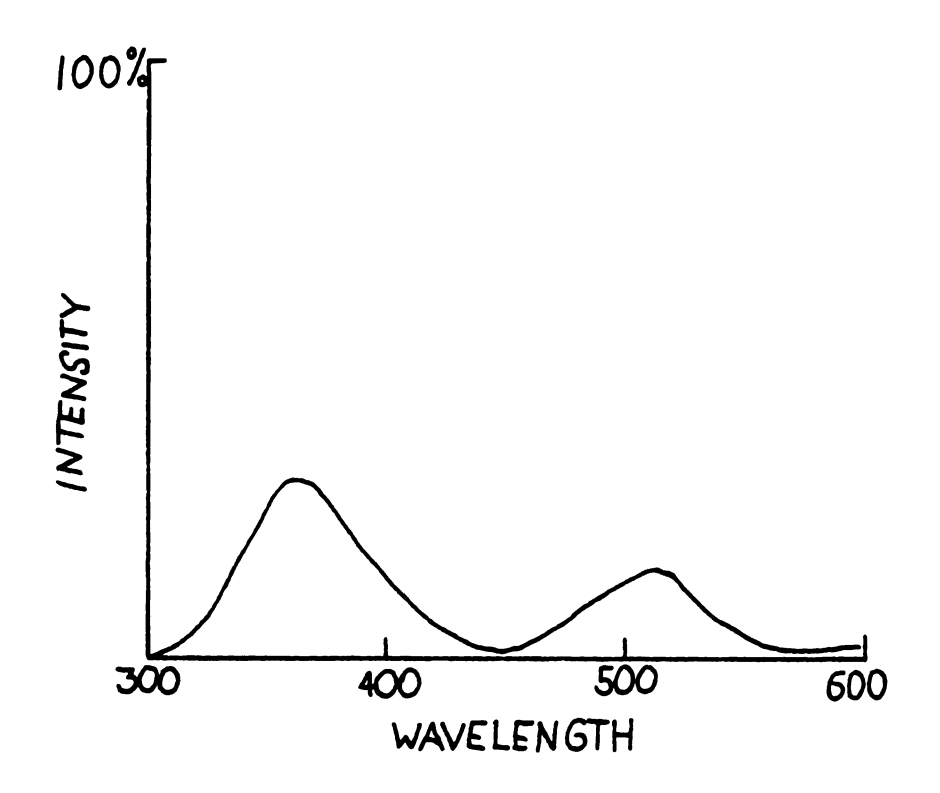


Figure 43. Fluorescence spectrum of tryptophanase in potassium

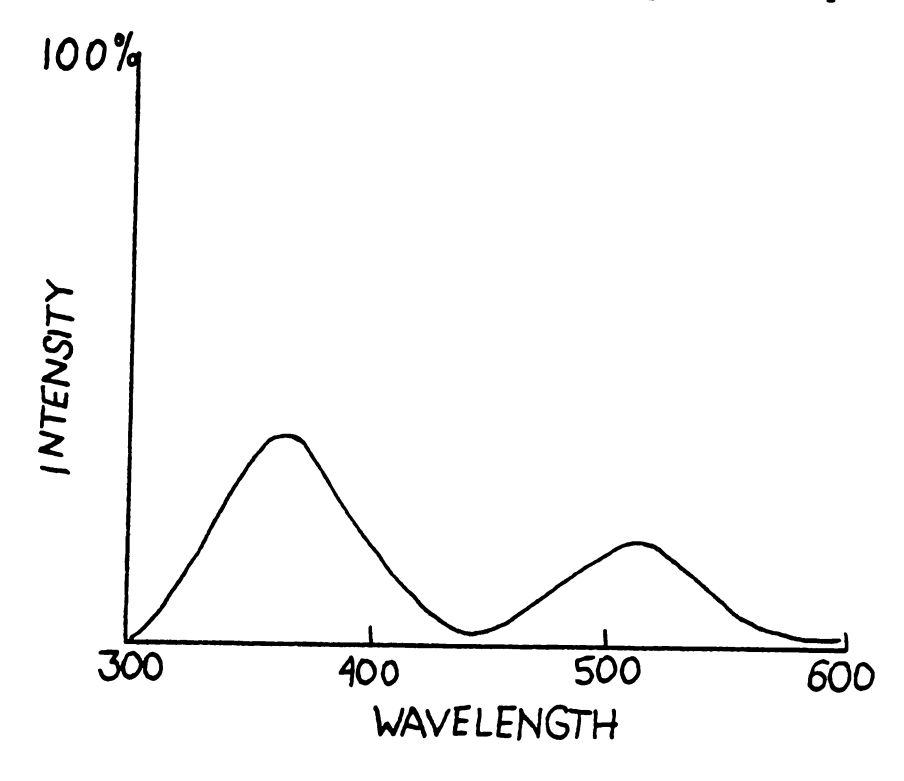


Figure 44. Fluorescence spectrum of tryptophanase in rubidium

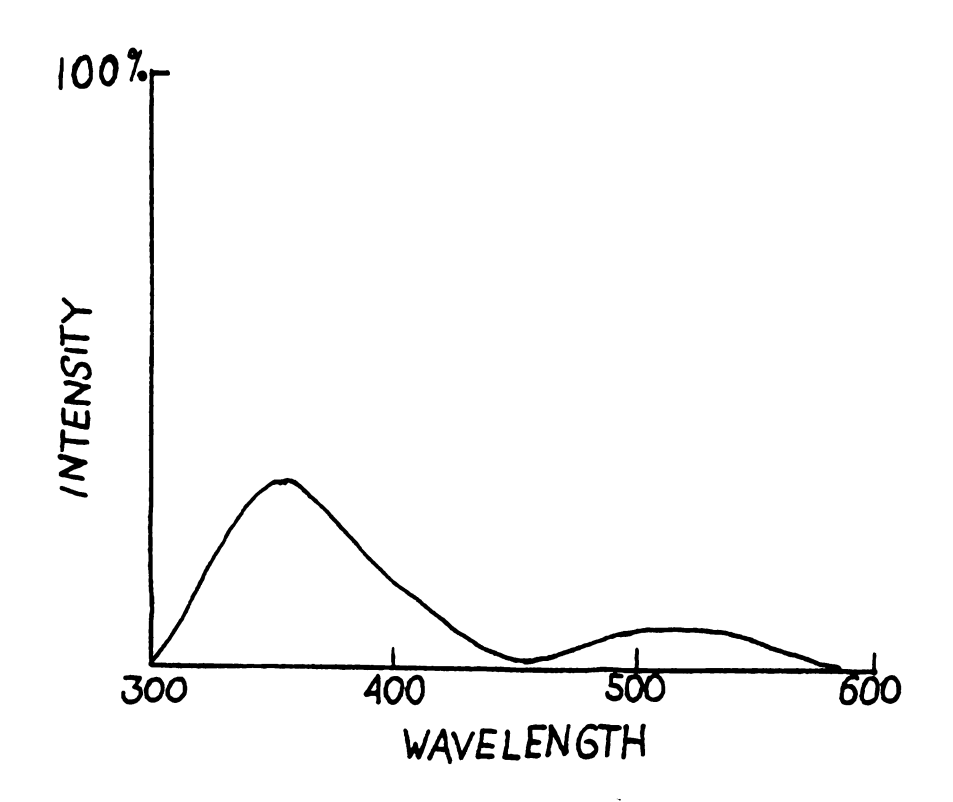


Figure 45. Fluorescence spectrum of tryptophanase in lithium

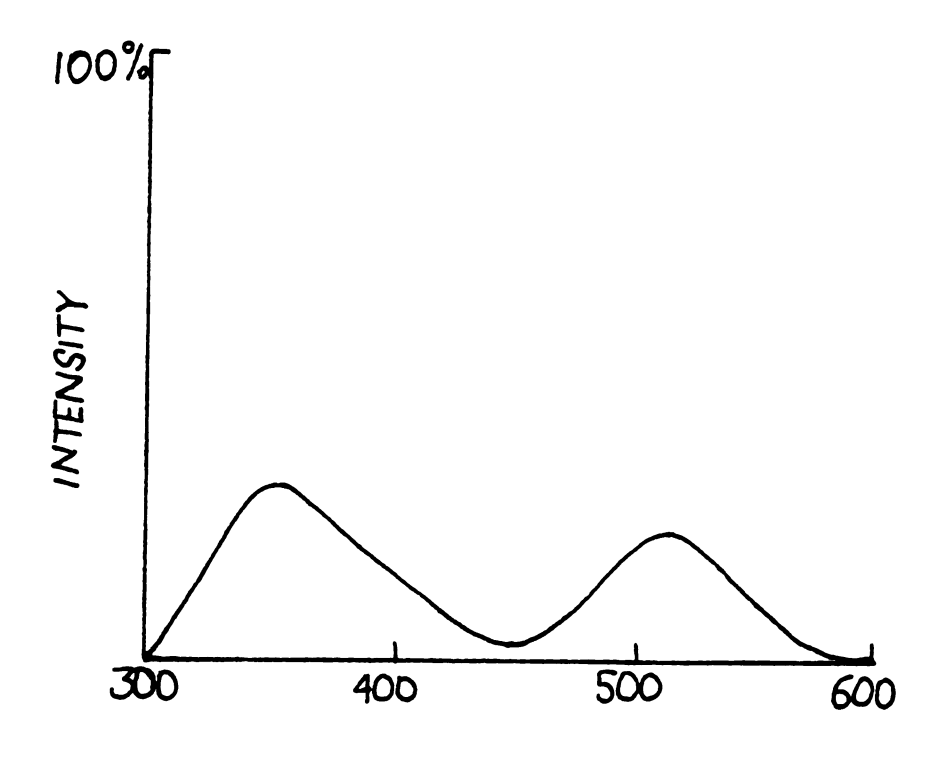


Figure 46. Fluorescence spectrum of tryptophanase in cesium

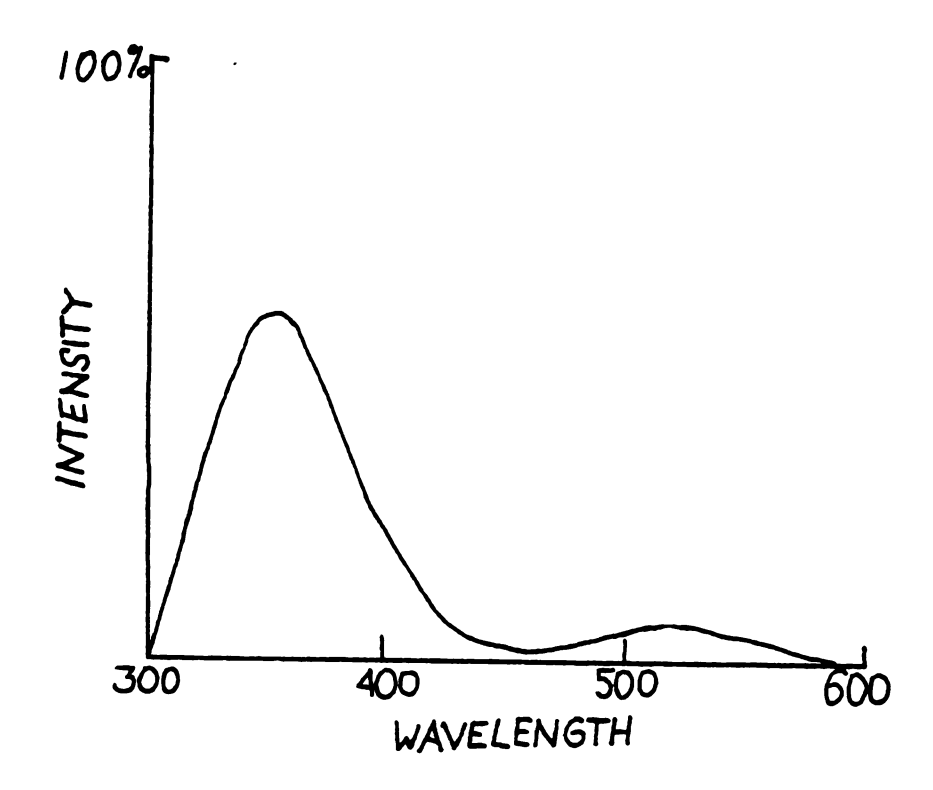


Figure 47. Fluorescence spectrum of tryptophanase in sodium

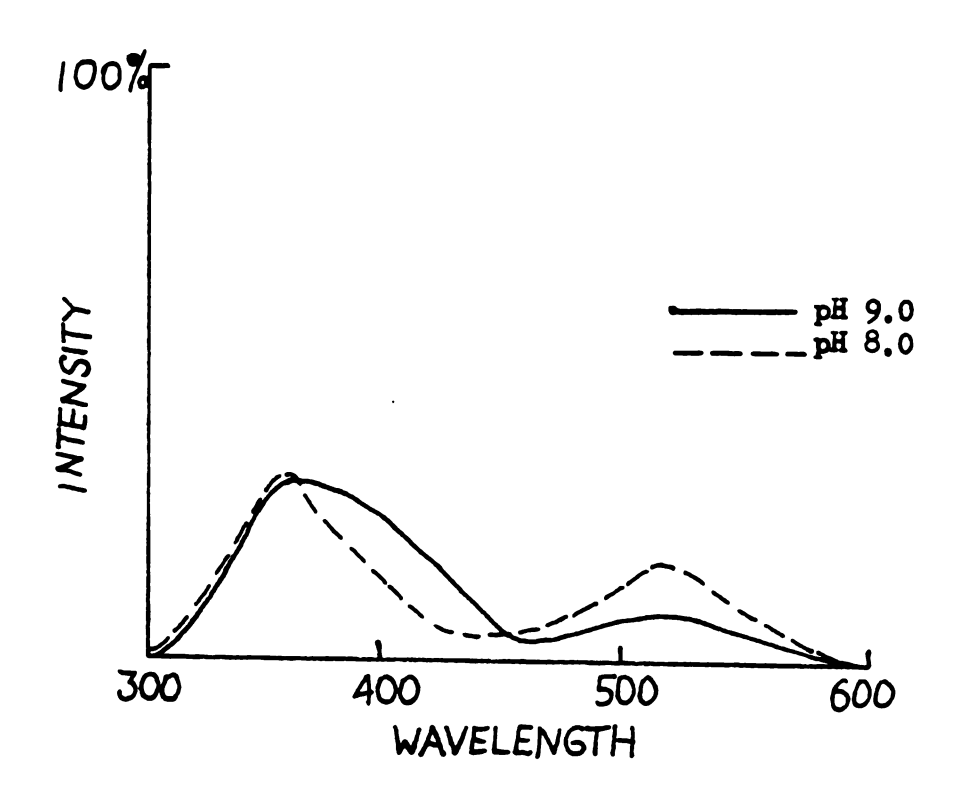


Figure 48. Fluorescence spectra of tryptophanase in potassium

respectively. It is difficult to demonstrate the 400 nm emission directly by exciting at 337 nm because of the emission of the free pyridoxal-P in equilibrium with the enzyme, but its existence can be demonstrated by overlaying the fluorescence spectrum of the apoenzyme, Figure 31, and that of the holoenzyme in potassium phosphate, Figure 35, both at pH 8.0. One can readily see that in the latter spectrum there is additional intensity on the long wavelength side of the 350 nm peak. The holoenzyme in potassium phosphate exhibits a large 337 nm absorption at this pH, to which this 400 nm emission can be attributed.

Another instance of this additional intensity may be seen in Figure 48, comparing holoenzyme in the presence of potassium at pH 8.0 and pH 9.0. The increase in fluorescence intensity at 400 nm can be correlated with the increase in the 337 nm band in the absorption spectrum which occurs upon increasing the pH.

There remains the question of why the 400 mm and 510 mm emissions are excited when the holoenzyme is excited at 280 nm. Several possibilities exist. Clearly, the emission of the apoenzyme is quenched upon binding of pyridoxal-P. Since the 350 nm from the protein tryptophan residues strongly overlaps the absorption of the 337 nm form of bound pyridoxal-P, one might propose nonradiative energy transfer with tryptophan as donor and the 337 nm form of pyridoxal-P as acceptor, emission being observed from the latter, as an explanation for the 400 nm emission. Direct excitation of the 337 nm form at 280 nm is also possible but model compounds absorbing near 337 nm tend to absorb weakly at 280 nm, with a high energy absorption maximum near 250 nm.

In the case of the 510 nm emission, the corresponding 420 nm absorption does not overlap the emission of tryptophan. There is an

overlap with the 400 mm emission arising from 337 mm bound pyridoxal-P but these forms occur on different protein subunits and distances might well be too great for efficient transfer of energy. In model compounds. the forms absorbing near 420 nm often have a 280 nm absorption maximum so that the 510 nm emission might be a result of direct excitation of the 420 nm form of bound pyridoxal-P. However, the 510 nm emission is also observed when the holoenzyme is excited in the 310-380 nm region where the 420 nm form absorbs very little. For this reason, and based on the photophysical behavior of orthohydroxyaldehydes and orthohydroxyazomethines 18. a possible explanation for at least part of the 510 nm emission is proton transfer in the excited state. When the 337 nm form is excited, directly or via energy transfer, a proton can be accepted by the imine nitrogen of the enzyme bound Schiff's base, resulting in interconversion to the excited 420 nm form. If the rate of this process is fast enough for the reaction to occur appreciably during the lifetime of the excited state, emission can be observed at 510 nm. Proof of this hypothesis could be obtained by an analysis of fluorescence lifetime data; this topic will be discussed in the section of this chapter devoted to fluorescene lifetime studies.

Examining the fluorescence spectra as a function of monovalent cation, one notices the similarity between the spectra in the presence of potassium and of rubidium. However, there is a significant increase in the 510 mm emission in the case of ammonium, the other cation that activates well. This is the opposite effect from what might be expected on the basis of the 337/420 nm ratio which is greater in the presence of ammonium than in the presence of the other two cations. Therefore, it is possible that ammonium acts to shift the equilibrium in the excited

state toward the proton transferred species and consequently toward the 510 nm emission; however, it is also possible that there exists some change in the emitting species since there is also a shift in absorption spectrum.

In the case of the fluorescence spectra of the poorly activating cations lithium, cesium, and sodium, one sees a blue shift of the 350 mm band that can be attributed to the loss of the 400 nm contribution. This fact is consistent with the disappearance of the 337 nm band in the absorption spectra. In addition, the sodium sample shows a very high 350 nm peak which may be explained if part of the enzyme is in the apoensyme form with a higher quantum yield of fluorescence; this diminished binding of pyridoxal-P also explains the decrease of the 510 nm emission which is observed with sodium.

The cesium sample shows an increased 510 nm emission as expected on the basis of the increased 420 nm absorption. As in the case of absorption, the fluorescence spectrum of tryptophanase in the presence of lithium is anomalous. The decrease in the 510 nm band might be explained by some characteristic of the cation which decreases proton transfer in the excited state. Alternatively, there may be a difference in the ground state since the absorption spectum shows changes in maximum wavelength of absorption.

B. FLUORESCENCE LIFETIME STUDIES

The fluorescence lifetime τ is an important photophysical parameter whose measurement may be accomplished by single photon counting techniques. Lewis et al. 43 discuss the manner in which the true decay function G(t) can be obtained from experimental data by solution of the integral equation

$$D(t) = \int_{0}^{t} I(t-\lambda) G(t) d\lambda$$

where D(t) is the experimental decay curve and I(t) is the experimental lamp curve measured under identical conditions. In general, extracting lifetimes of less than 10 nsec. requires careful attention to the mathematical method. In addition, I(t) is wavelength dependent due to variations in the lamp time characteristics and the spread of photomultiplier transit times. These effects may introduce complications into analysis of decays of less than about 2 nsec.

Ware et al. The review various deconvolution methods and point out the importance for certain applications of being able to recover the true decay law without a priori assumptions of its functional form. The method that they advocate is to represent G(t) as a general sum of exponentials

$$G(t) = \sum_{k=1}^{n} a_k e^{-t/\gamma_k}$$

The problem is linearized by preselection of the δ_k 's, varying only the a_k 's. The number of exponentials n is chosen sufficiently large that G(t) is flexible enough to fit a wide variety of decays, with no physical significance being attributed to the δ_k 's or a_k 's. Once G(t) has

been obtained, it is possible to compare this function to various decay laws. Ware et al. have implemented the preceding analysis along with a least squares analysis of G(t) according to a one or two exponential decay law in a computer program which is used routinely in this laboratory after being obtained from Dr. William Ware.

Ware et al. that the criterion of success for their method is the smoothness of G(t) and also the sum of the squares of the residuals between experimental points and points generated by convolution of G(t) with the experimental lamp curve. Reasons for a poor fit may include poor choice of the δ_k 's, poor data, or too short a lifetime. In addition, the integral equation itself may fail.

In a recent paper, Lyke and Ware discuss deconvolution of very short fluorescence lifetimes. Data analysis is carried out by nonlinear least squares assuming a sum of exponentials for G(t). Computer programs implementing this method have been obtained from Dr. William Ware and Dr. Ludwig Brand and modified for use in this laboratory.

The analysis of fluorescence decays by the method of nonlinear least squares is developed extensively by Grinvald and Steinberg. 46

They argue, after Knight and Selinger, that the preferred method of deconvolution assumes a functional form for G(t) with adjustable parameters, often a sum of exponentials. Goodness of fit is judged by the sum of the squares of the weighted residuals, with the correct weights being given by a Poisson distribution in the case of single photon counting data.

A feature of the nonlinear least squares program of Dr. Ludwig Brand is the use of a lamp shift correction, discussed by Gafni et al. 48 The energy dependence of the photomultiplier transit time introduces a distortion in the profile of the lamp which these authors claim may be approximated by a relative time shift between the experimental data and lamp curves. In this laboratory the lamp curve was shifted by a spline function interpolation program supplied by Thomas H. Pierce.

Other methods of determining a proper lamp profile have been proposed. Britten and Lockwood make use of two reference compounds, A and B. The equation

$$I'(t) = I(t) + \gamma_{A} \frac{dI(t)}{dt}$$

is used to calculate the corrected lamp curve I'(t) from a range of possible values of \mathcal{T}_A , the fluorescence lifetime of compound A. The I'(t) that best calculates the lifetime of standard B as judged by the residuals is then used in analyzing lifetime data of the sample of interest. Wong and Halpern describe a method of attenuating the tail region of the experimental lamp curve in order to better analyze short lifetimes.

A ratio correction technique for the variation of the photomultiplier time response with wavelength is presented by Rayner et al. 51 These investigators propose alternate collection of the experimental data and lamp curves with the decay curves of a fluorescence standard selected for high fluorescence yield, short lifetime, and fluorescence spectrum spanning the excitation and emission wavelengths of the sample. The decay curves for the standard are measured at both of these wavelengths and mathematical analysis yields corrected data and lamp curves to which deconvolution procedures may be applied.

McKinnon et al. 53 report computational performance tests of seven deconvolution methods. The method of Ware et al. 44 was rejected as being

unable to tolerate even low levels of noise added to simulated double exponential decay data. The method of Grinvald and Steinberg 46 was judged best in its ability to obtain correct values in spite of noise and closely spaced lifetimes.

The fluorescence decay curve of 9-cyanoanthracene in cyclohexane is suggested by Gani et al. 48 as a test of the deconvolution procedure for nonlinear least squares analysis. In the present work, the best fit of the 9-cyanoanthracene lifetime is used to determine a value for the lamp shift correction. In Figure 49 is shown a plot of the fluorescence decay of 9-cyanoanthracene observed at 450 nm upon excitation at 340 nm, together with the curve obtained upon convoluting the lamp with the best fit single exponential.

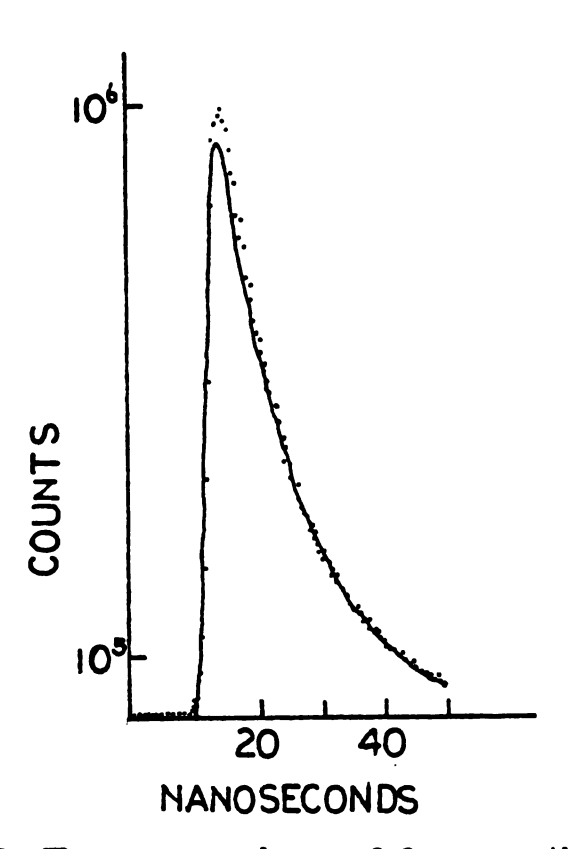


Figure 49. Fluorescence decay of 9-cyanoanthracene

The experimental lamp curve was interpolated and shifted various amounts between zero and two channels (0.383 nsec./channel) and the values of the lifetime τ , preexponential a, and χ^2 were calculated Results are tabulated in Table 3.

Table 3. Lamp shift corrections

	<i>y</i>		
Lamp shift		7	x2
0.000	0.0545	11.45	24.35
0.200	0.0565	11.10	5.866
0.285	0.0572	11.00	3.856
0.290	0.0572	10.99	3.845
0.295	0.0572	10.98	3.852
0.300	0.0573	10.93	3.879
0.325	0.0 <i>5</i> 7 <i>5</i>	10.89	4.189
0.383	0. 0578	10.81	6.200
0.766	0.0591	10.40	51.14

The fluorescence decay curve for holotryptophanase in TMA-EPPS, pH 8.0, containing 0.15 M KCl and excited in the 320-380 nm region was measured at 420 nm and 510 nm as shown in Figures 50 and 51. Attempts to deconvolute these data by the method of Ware et al. $^{\mu\mu}$ failed because of oscillations in G(t). In Tables 4 and 5 are tabulated the values of preexponential factors and lifetimes for a nonlinear least squares analysis of the 510 nm data. Two exponentials are assumed and the calculations are performed without lamp shift correction and with a lamp shift correction of 0.275 nsec; in the latter, there is a large improvement in χ^2 and large changes in the parameters.

As discussed previously, these data are something of a worst case

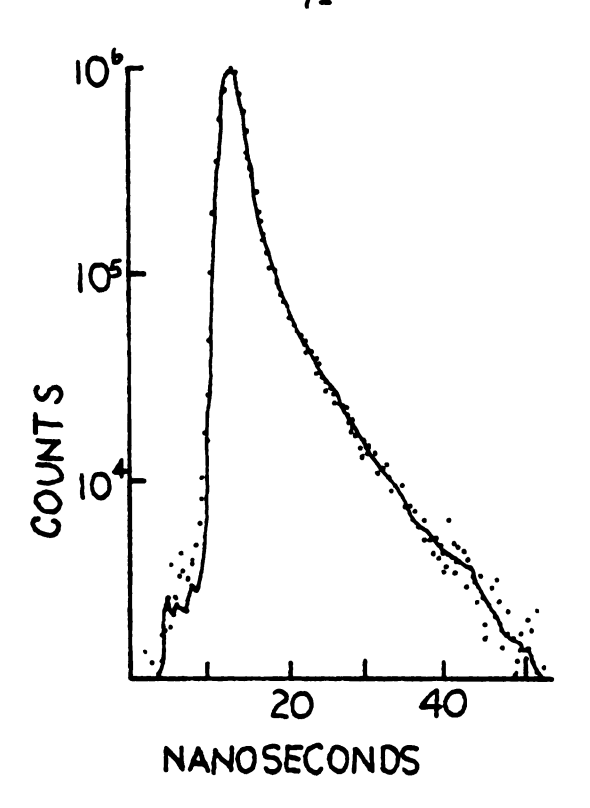


Figure 50. Fluorescence decay of tryptophanase, 420 mm

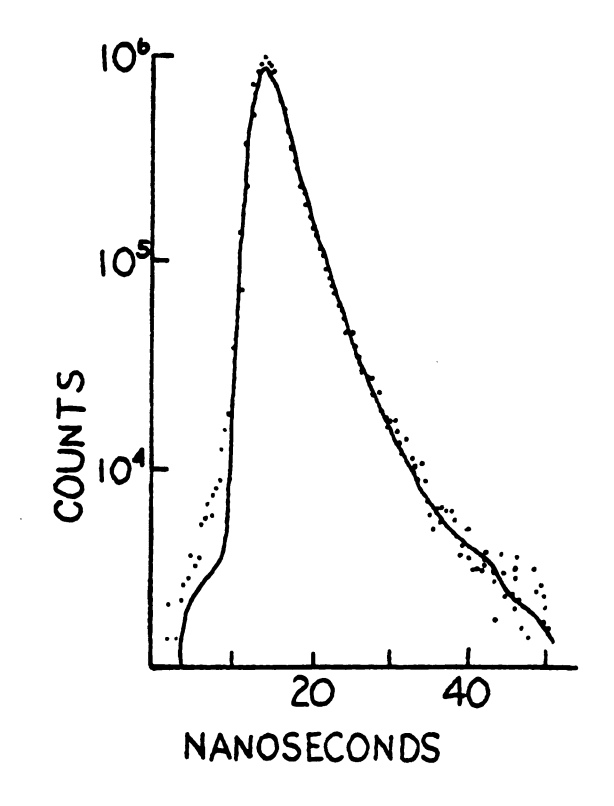


Figure 51. Fluorescence decay of tryptophanase, 510 mm

Table 4. Decay parameters

a 1		a 2			
0.111	2.71	0.002	8.81	9.04	
0.087	2.78	0.001	10.7	8.02	

Table 5. Decay parameters with lamp shifted

a 1		a 2		
0.089	1.29	0.058	3.44	8.35
0.095	2.08	0.011	5.66	5.01

for this method of analysis because of the short, close together lifetimes and these results cannot be considered to be definitive. However, it can be stated that there are probably two components to the decay with one lifetime of 1 to 2 nsec. and a second of 3 to 6 nsec.

Analysis of the 420 nm decay is further complicated by the presence of scattered light. The data can be fitted with the following expression

$$G(t) = 2.02 \exp(-t/0.321) + 0.170 \exp(-t/2.10) + 0.034 \exp(-t/7.00)$$

The first component of the decay is due to scattered light whose lifetime departs from zero because of the lamp shift. An attempt to correct for lamp shift in this analysis led to a divergence of the method as the short lifetime approached zero.

Short lifetimes for the bound forms of pyridoxal-P are not unexpected considering the short lifetimes of free pyridoxal-P. An improvement in the results presented here might be brought about by the method of Rayner et al. which, however, uses a more complicated system of collecting data than is presently available in this laboratory. Better

meters for the investigation of changes in the enzyme due to buffers, monovalent cations, etc. Analysis of lifetime data could also give a direct proof of the existence of excited state proton transfer in pyridoxal-P enzymes, the possibility of which has been argued from the results of studies of model compounds up to now.

C. KINETIC STUDIES

Kinetic studies on tryptophanase were performed in collaboration with a group of investigators studying the structural and functional aspects of enzymes as deduced by static, dynamic, and theoretical methods. Other members of the group during the course of this study have included D.S. June and C.H. Suelter, Biochemistry Department; T.H. Pierce, R. Cochran, S.V. Elias, F. Halaka, I. Behbahani-Nejad, F.H. Horne, and J.L. Dye, Chemistry Department; and M.A. El-Bayoumi, Biophysics and Chemistry Departments.

It is known that there is a conformational difference between holo-tryptophanase in the presence of sodium and holotryptophanase in the presence of potassium. 29 Such a conformational change might be associated with coenzyme rotation as is discussed in connection with the model developed in Chapter 3. Since decreasing the pH and removing activating monovalent cations appear to have similar effects on the absorption spectrum of the enzyme, one might also expect changes in conformation with pH. All of these considerations, as well as analysis of the enzyme reaction mechanism, suggested the desirability of observing the effects on the absorption spectrum of sudden changes in pH or monovalent cation.

June et al.⁵³ performed three rapid scanning stopped flow studies of the effect on holotryptophanase of a change in pH or potassium concentration. In each of these experiments there was a clear observation of a slow process in which a 420 nm absorbing form disappeared and a 337 nm form appeared, or vice versa.

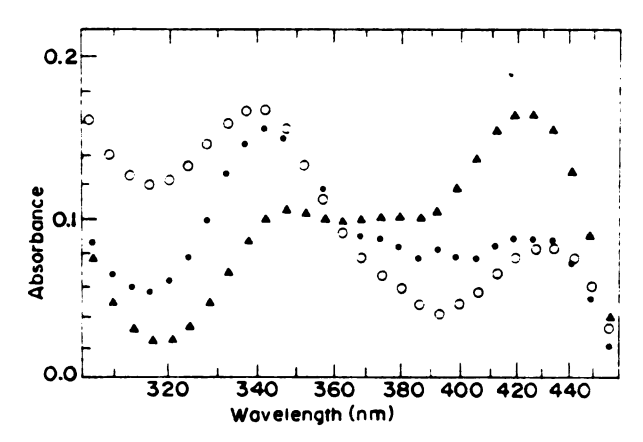
In the pH drop experiment (pH 8.53 to pH 6.72), interconversion of the 337 nm and 420 nm absorbances follows a first order decay for the 337 nm band and first order growth of the 420 nm band fellowing a rapid drop of pH. Initial (abrupt) changes occur within the mixing time of the instrument (about 6.5 msec.), as evidenced by differences between the initial enzyme spectrum and a spectrum which has been synthesized to represent the enzyme just after mixing.

Upon raising the pH from 7.38 to 9.30, the 420 nm and 337 nm forms also appear to interconvert at a similar rate. There are some very fast changes as well as a very slow process in which absorbance decreases at 325 and 425 nm and increases at 360 nm. The fact that these last spectral changes resemble a difference spectrum between bound and free pyridoxal-P forms, a process that might well occur if pyridoxal-P binding were pH dependent, suggests that holoansyme-apoensyme interconversion may account for all or part of the very slow process.

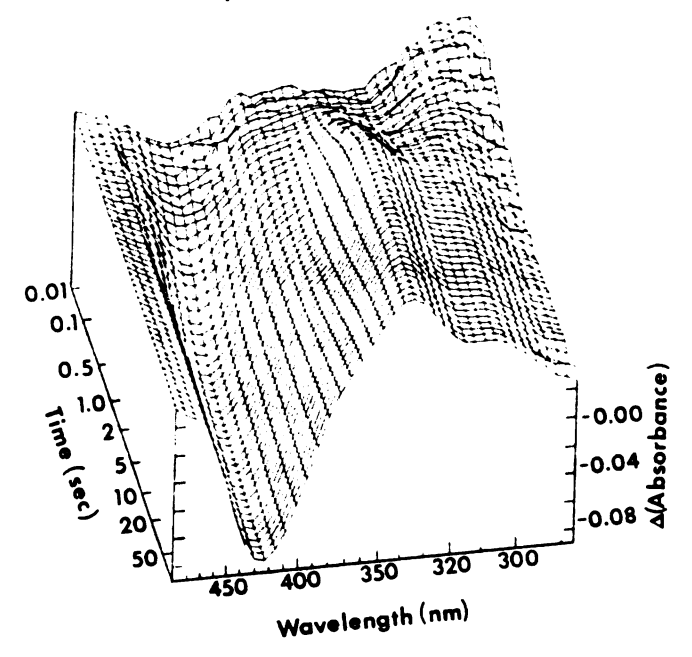
The third experiment involved the exchange of potassium for sodium in a sample of holoenzyme. Since K_D for sodium binding to the enzyme is about 40 mM and for potassium is 1.4 mM, cation exchange can be effected by mixing equal volumes of identical concentrations, as demonstrated by a calculation of reaction velocity attainable in this situation. Using the equation for competitive inhibition (as suggested by C.H. Suelter)

$$\frac{1}{v} = \frac{1}{v} + \frac{K_K^+}{v [K^+]} \left(1 + \frac{[Na^+]}{K_{Na}^+}\right)$$

where v is the expected velocity, V is the maximum velocity (observed in the presence of K^+ alone, K_M^+ is the dissociation constant for M^+ , and $[M^+]$ is the concentration of the cation M^+ , one can calculate the value V = 0.94 V for 50 mM final concentration of each cation. This can be achieved by making up the enzyme in 100 mM sodium and mixing it with



Tryptophanase spectra (path length 1.85 cm) corrected for free pyridoxal-P absorption, observed in the pH drop experiment: zero time, O; first spectrum after mixing (t = 6-12 ms), \bullet ; spectrum after completion of the first-order process (t = 8 s), \triangle .



Absorbance difference-wavelength-time surface observed in the pH jump experiment. The spectra of free pyridoxal-P and of trypto-phanase at zero time $(\mathcal{A}_0(\lambda))$ have been substracted to give these difference spectra.

Figure 52. pH drop and pH jump 53

a solution containing 100 mM potassium.

A concentration of 80 M pyridoxal-P in the enzyme sample was near the maximum value feasible for use in the stopped flow apparatus. As was shown earlier, tryptophanase in 100 M pyridoxal-P may not be completely saturated with coenzyme. Therefore, effects of additional pyridoxal-P binding to the enzyme when potassium is added are likely to be observed if they occur on a time scale similar to the other processes, i.e., interconversion of free and bound forms cannot be cleanly separated from interconversion of bound forms.

This 'potassium jump' experiment clearly showed the slow 420 nm to 337 nm interconversion with approximately the same rate as in the pH change experiments. Figure 53 is an absorbance-wavelength-time surface generated by computer for this experiment. Figure 54 shows the first spectrum taken after mixing and the last spectrum taken 68 sec later. Figures 55 and 56 show the time cuts of the absorbance at 337 nm and 420 nm, respectively. These changes follow rate laws more complex than first order.

A preliminary investigation of the rate of pyridoxal-P binding to the apoenzyme is shown in Figure 57. These data demonstrate that the rate of binding in the buffers used for pH change stopped flow experiis much faster than the rate in potassium phosphate buffer that has been used to study binding. This result confirms the idea that binding effects may well be a factor in experiments in which pH or monovalent cation is changed.

It is important to add the fact that much closely related research on tryptophanase has been carried out by members of the enzyme group since the time I concluded my work and began writing this dissertation.

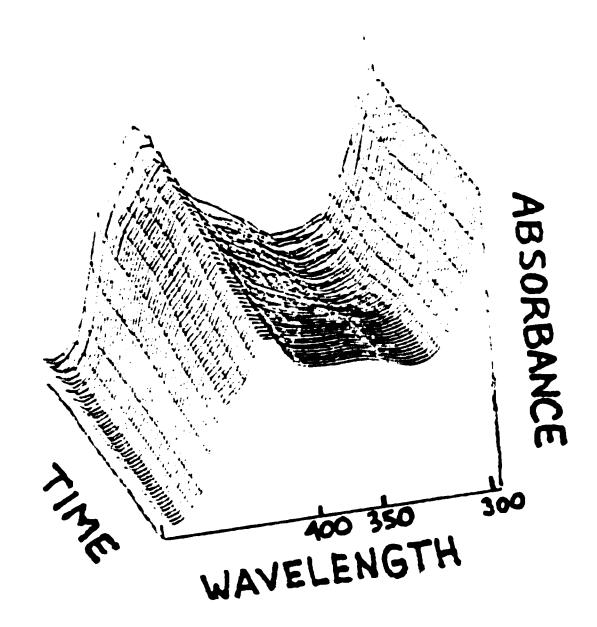


Figure 53. Absorbance-wavelength-time surface

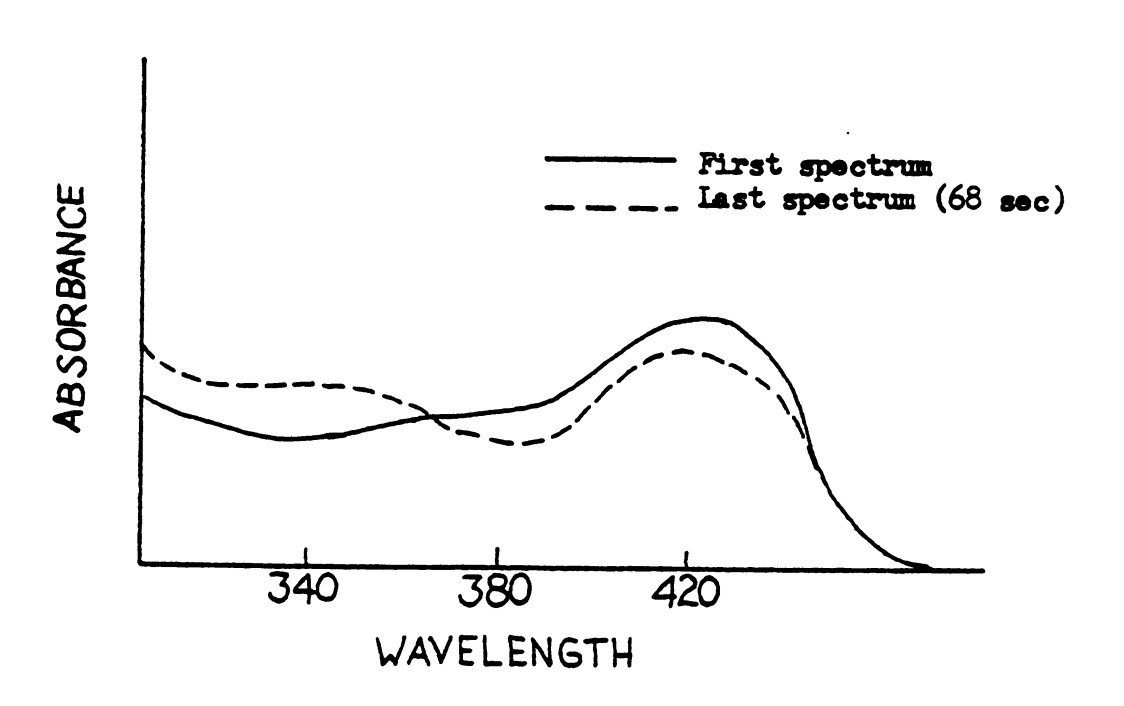


Figure 54. First and last spectra

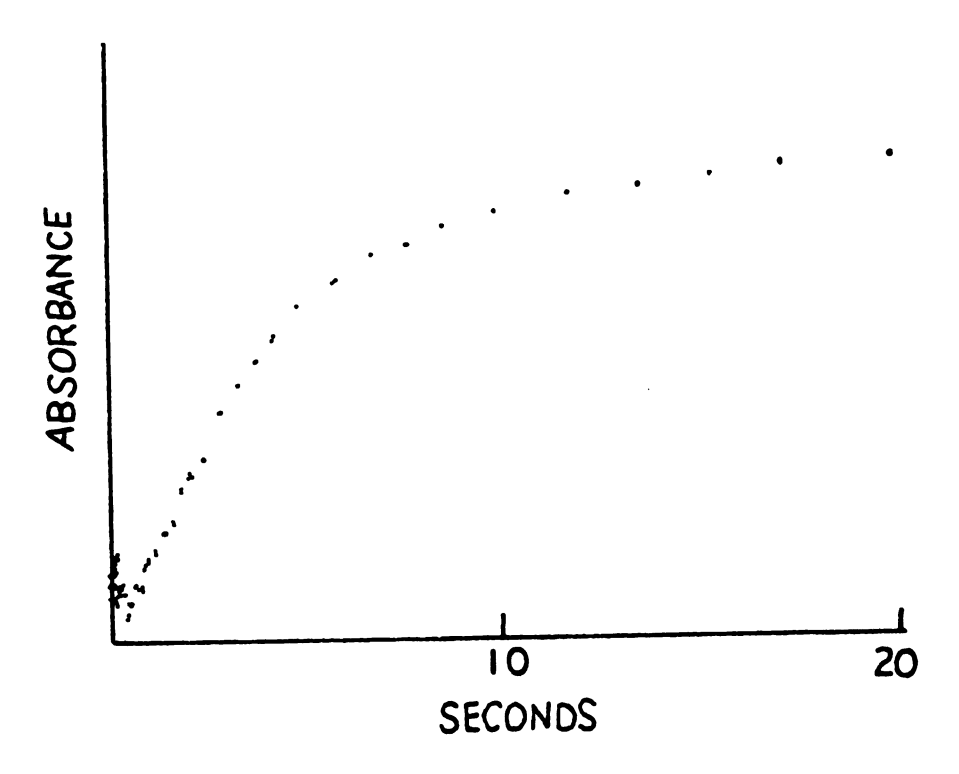


Figure 55. Time cut at 337 mm

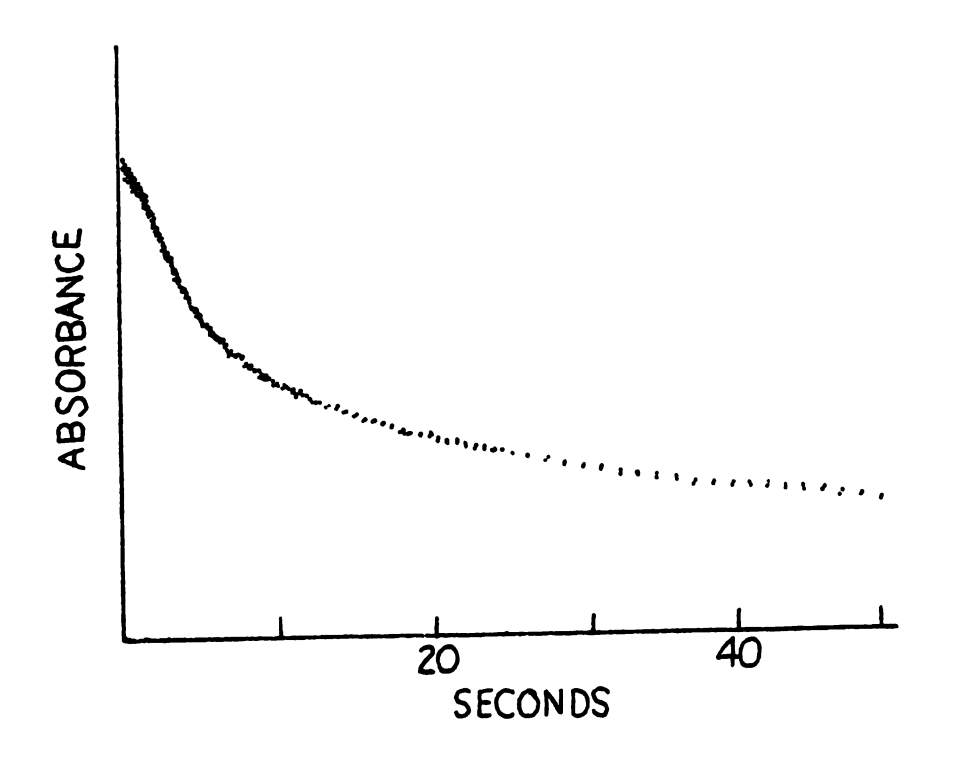


Figure 56. Time cut at 420 nm

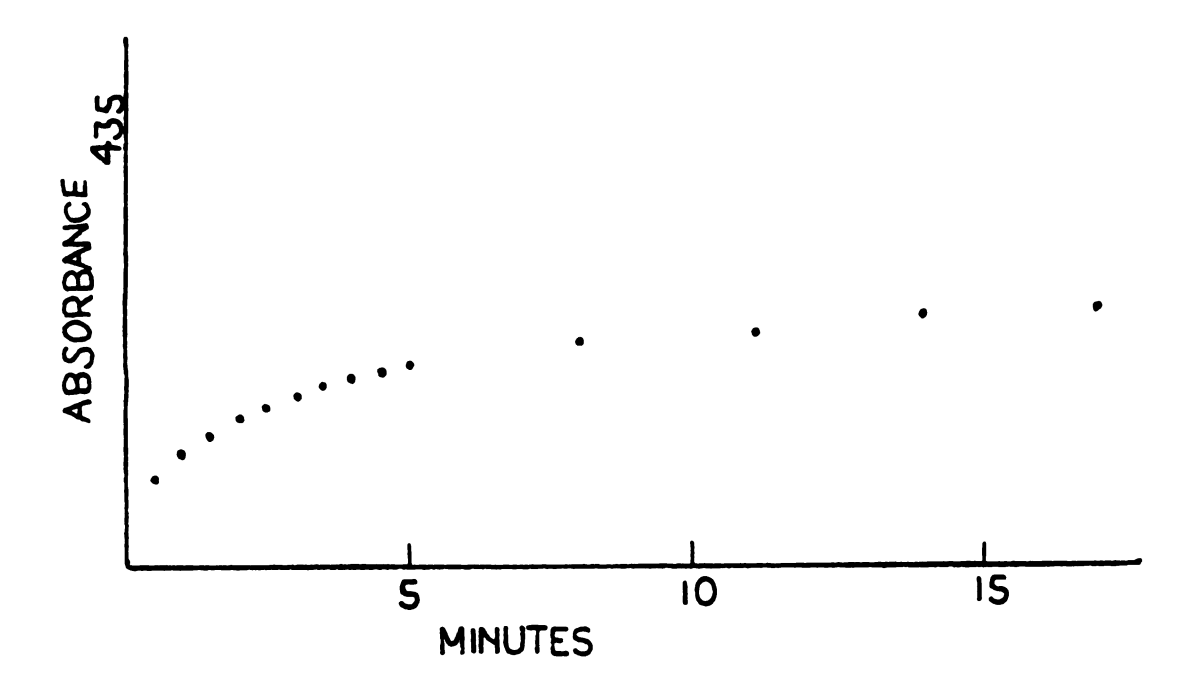


Figure 57. Pyridoxal-P binding to apotryptophanase

CHAPTER 5

MATERIALS AND METHODS

A. GROWTH OF E. COLI B/1t7a

E. coli B/1t7a is a mutant of E. coli strain B which is constitutive for tryptophanase. Cultures were maintained on plates and slants of minimal agar.

minimal agar, 300 ml.

KH_PO4 0.9 g.

K2HPO4 2.2 g.

 $(NE_4)_2 SO_4$ 0.3 g.

bactoagar 5.4 g.

After autoclaving, add separately autoclaved

indole (1 mg/ml) 3 ml.

glucose (30 mg/ml) 10 ml.

and filter sterilized minerals, 1 ml.

minerals, 100 ml

CaCl₂'2H₂O 0.03 g. MgSO₄'7H₂O 3 g.

FeSO₄ '7H₂0 0.03 g.

In order to grow starting materials for the preparation of tryptophanase, a 10 ml. culture of nutrient medium was innoculated from a single colony obtained from a culture streaked on minimal agar.

mutrient media, 11.

casein hydrolysate	10 g.	KH ₂ PO ₄	7.5 g.
yeast extract	0.1 g.	K2HPO4	16.5 g.
bactotryptone	10 g.	(NH ₄) ₂ SO ₄	1 g.

After autoclaving, add separately autoclaved

and filter sterilized

minerals 1 ml.

L-tryptophan (10 mg/ml) 3.4ml.

minerals, 100 ml.

CaCl 2.5H 0	0.03 g.	ZnS0 ₄ • 7H ₂ 0	0.01 g.
FeSO4 '7H20	0.03 g.	Cuso ₄ • 5H ₂ 0	0.01 g.
MgS04 7H20	3 g.	Na.Cl	2.5 g.
MnSO4 .7H20	0.01 g.		

Successive innoculations of the entire culture were made into 100 ml., 5 l. and 100 l. volumes, with growth times of approximately 12 hr. into stationary phase. The 100 l. culture was harvested by centrifugation at an optical density at 660 nm of 4.92 with a yield of 197.7 g of wet weight of cells, which was frozen in 30 g portions for up to three months before being subjected to purification.

Cells were grown with 100 rpm mixing to prevent sedimentation and a slow rate of aeration. A typical yield of \underline{E} , coli in an anaerobic culture is about 150 g , whereas under aerobic conditions the yield may be more like 450 g. The nearly anaerobic growth conditions are apparently important for the maximum production of tryptophanase and we have generally found that the higher the total

cell wet weight harvested, the lower amount of tryptophanase per 30 g. of starting material.

B. PREPARATION OF THE SEPHAROSE COLUMN

Ligands are coupled to Sepharose by cyanogen bromide in a procedure adapted from that of Shaltiel and Er-el;

- 1. Dissolve 15 g. of cyanogen bromide in a small volume of p-dioxane.
- 2. Dissolve 75 g. of 1,7-diaminoheptane in 300 ml. of H₂0; adjust pH to approximately 9.5.
- 3. Wash 150 g. of Sepharose 4B with 5 volumes of H₂0. Resuspend in a total volume of 300 ml.
- 4. Add the cyanogen bromide to the Sepharose with stirring.

 Maintain the pH at 11.
- 5. After 8 min., stop the reaction by the addition of ice.
- 6, Wash with 1 l. of H_2 0. Resuspend in 300 ml. 0.1 M NaHCO₃.
- 7. Immediately add the 1,7-diaminoheptane with stirring; adjust the pH to 9.5.
- 8. Stir overnight at room temperature.
- 9. Wash with H_2 0, 0.1 M NaHCO₃, 0.05 M NaOH, H_2 0, 0.1 M CH₃COOH, and H_2 0.

The Sepharose column is stored in the cold in the presence of 0.02 % sodium azide as a preservative between purifications of the enzyme. It is regenerated with washes of NaOH, H_2O , HCl, and H_2O , followed by adjusting the pH to 7.0. An earlier version of this column was made with only half as much ligand as above. The column

failed to purify tryptophanase properly and this fact explains the report by Suelter et al. that it was necessary to add a DEAE column to the purification scheme. Also, we have observed the column to fail from time to time and in an attempt to protect the Sephanose we have made the regeneration procedures more gentle by decreasing the acid and base concentrations from 0.5 M to 0.2 M. Column material that has failed can be observed to stick to glass or even to form lumps.

C. PURIFICATION OF TRYPTOPHANASE

The purification procedure is adapted from the procedure of Suelter et al. 40

Step 1, 30 g. wet weight of cells of \underline{E} , $\underline{\operatorname{coli}} \cdot B/1t7a$ were suspended in 150 ml. of cold Buffer A and treated on ice by sonication for three 3 min. cooling periods between. Cell debris was removed by centrifugation.

Step 2. The supernatant from Step 1 was diluted with Buffer A to a protein concentration of 10 mg/ml, as determined by the method of Warburg and Christian, and adjusted to pH 6.0 with 10 % acetic acid.. Nucleic acids were precipitated by the addition of one fifth volume of 2 % protamine sulfate, followed by stirring at room temperarure and centrifugation.

Step 3. The supernatant solution from Step 2 was adjusted to pH 7.0 with 10 % NH_{μ}OH. Solid (NH_{μ})₂SO_{μ} (24.8 g/100 ml) was added gradually with stirring over a 30 min period on ice, with the pH maintained at 7.0 with NH_{μ}OH. After removing the precipitate by centrifugation, solid (NH_{μ})₂SO_{μ} (15.6 g/ml) was added in the same fashion.

The precipitate was collected by centrifugation, dissolved in a minimum volume of Buffer B, and adjusted to one-third the volume of the supermatant solution from Step 2. One-hundred ml. portions were heated to 65°C in a 72°C water bath and kept at this temperature for 5 min. The denatured protein was removed by centrifugation. Step 4. The supermatant solution from Step 3 was made 60 \$ saturated in $(NH_{L})_2SO_L$ by addition of 25 g/ 100 ml gradually with stirring over a 30 min period on ice. The precipitate obtained by centrifugation was dissolved in a minimum volume of Buffer C and dialyzed against two changes of 1 1. of Buffer C overnight.. Step 5. The dialyzed solution from Step 4 was applied at room temperature to a Seph-C₂-NH₂ column (2,5x40 cm) equilibrated with Buffer C. The column was washed with Buffer C to remove nonadsorbed protein. At this point, monitoring at 280 nm and collection of fractions of the effluent was begun in order to be able to save the enzyme should it fail to stick to the column. Tryptophanase was eluted with a 1000 ml linear gradient composed of 500 ml of Buffer C and 500 ml of Buffer C containing 0.2 M NH_{LL}Cl. Tryptophanase elutes at 0.13-0.15 M NH_LCl.

Step 6. Active fractions from the Sepharose column were pooled and dialyzed overnight against Buffer D. If apoenzyme was desired, the enzyme solution was made 10 mM in penicillamine before dialysis.. The precipitated material in the dialysos bag is centrifuged and resuspended in a minimum volume of Buffer D. Tryptophanase may be stored in this manner in the refrigerator for several months; additional sulfhydryl compounds may be added from time to time.

One can isolate as much as 300 mg of tryptophanase by the preceding procedure, although the dialyzed solution from Step 4 needed to be split and half and the Sephanose column run twice. This high yield was attributed to a particularly good batch of E. coli B/1t7a. On the other hand, a poor batch of bacteria and a failing column have yielded as little as 30 mg of tryptophanase, reproducibly, upon following the same procedure.

Buffer A, 500 ml.

potassium phasphate, pH 7.0. 1 M	50 ml
Na EDTA, 0.1 M	10 ml
dithiothreitol, 0.1 M	1 ml

Buffer B, 200 ml

potassium phosphate, pH 7.8, 1 M	20 ml
Na EDTA, 0.1 M	4 ml
pyridoxal-P, 20 mM	2 ml
(NH ₄) ₂ SO ₄ , solid	22 g
dithiothreitol, 0.1 M	2 ml

Buffer C, 11.

ammonium phosphate, pH 7.0, 1 M	25 ml
Na EDTA, 0.1 M	10 ml
glycerol, pure	100 ml
dithiothreitol, o.1 M	10 ml

Buffer D

potassium phosphate, pH 7.0, 1 M 100 ml

Na EDTA, 0.1 M	10 ml
(NH ₄) ₂ SO ₄ , solid	662 g
β -mercaptoethanol, pure	0.653ml
H ₂ 0	900 ml
Additional $(NH_{4})_{2}SO_{4}$ is added in the amount 66.2 g/ :	100 ml
of the volume in the dialysis bag (90 % saturation).	

D. BUFFERS FOR TRYPTOPHANASE

Titrate to pH 8.0 with T4A-OH

Activation buffer, 100 ml.

potassium phosphate, pH 8.0, 1 M	5 🛋
KCl, solid	0.75 g
Na EDTA, 0.1 M	2 ml
dithiothreitol, 0.1 M	1 ml
pyridoxal-P, 20 mM	0.5 ml
glycerol, pure	20 ml
25 mM TMA-EPPS buffer, 500 ml.	
N-2-hydroxyethylpiperazine propanesulfonic acid	3.15 g
EDTA, 0.1 M, titrated to pH 8.0 with tetramethyl-	
ammonium hydroxide (TMA-OH)	0.5 ml
dithiothreitol, 0.1 M	5 ml

25 mM TMA-phosphate buffer, 500 ml.	
phosphoric acid, concentrated	1.42 g.
EDTA, 0.1 M, titrated to pH 8.0 with TMA-OH	0.5 ml.
dithiothreitol, 0.1 M	5 ml.
Titrate to pH 8.0 with TMA-OH	
25 mM K-EPPS buffer, 500 ml	
N-2-hydroxyethylpiperasine propanesulfonic acid	3.15 g.
EDTA, titrated to pH 8.0 with TMA-OH	0.5 ml.
dithiothreitol, 0.1 M	5 ml.
KCl, solid	3.73 g.
Titrate to pH 8.0 with TMA-OH	
0.1 M potassium phosphate buffer, 500 ml.	
potassium phosphate, pH 8.0, 1 M	50 ml.
EDTA, 0.1 M, titrated to pH 8.0, 1 M	0.5 ml.
dithiothreitol, 0.1 M	5 ml.
(some preparation of sodium phosphate buffer)	•
5 mM TMA-EPPS containing cations, 100 ml.	
N-2-hydroxyethylpiperayine propanesulfonic acid	0.63 g.
EDTA, solid	0.029 g.
dithiothreitol, 0.1 M	1 ml.
cation	(table 2)
Titrate to pH 8.0 with TMA-OH	

5 mM TMA-CHES containing cations, 100 ml.

cyclohexylaminoethanesulfonic acid

0.104 g.

EDTA, solid

0.029 g.

dithiothreitol, 0.1 M

1 ml.

cation

(Table 2)

Titrate to pH 9.0 with TMA-OH

E. PREPARATION OF TETRAMETHYLAMMONIUM HYDROXIDE (TMA-OH)

- 1. Wash DOWEX 1x8, 20-50 mesh, with 0.1 M KOH
- 2. Pour column and wash with H₂0 untill effluent pH is 7.
- 3. Dissolve 4.38 g. of recrystallized TMAC1 in 40 ml of H₂0.
- 4. Apply TMA-Cl to column. Wash with H₂0 and monitor the pH of the effluent.
- 5. When effluent pH turns basic, collect 80 ml.

The resulting TMA-OH is about 0.5 M in concentration. It should be used immediately or stored frozen until use.

F. ENZYME ASSAY OF TRYPTOPHANASE

The pseudosubstrate S-o-nitrophenyl-L-cysteine (SOPC) was used for the spectrophotometric assay of tryptophanase activity. Suelter et al. 40 have shown that SOPC under goes d, β -elimination to give an o-nitrophenolate ion and that the reaction can be followed at 370 nm with a ΔE = 1860 liters mol⁻¹ cm⁻¹. The assay procedure involves preparing a cuvette containing 0.5 ml volumes of 0.1 M potassium phosphate buffer, pH 8.0, and 1.2 mM SOPC at

30°C. Typically the reaction is started with a few microliters of ensyme solution. The initial velocity is determined from the steepest part of the absorbance versus time curve and activity is calculated from the equation:

The specific activity es calculated by dividing the activity/ ml by the protein concentration in mg/ml. Suelter et al. report $\mathcal{E}_{200} = 0.795 \text{ mg ml}^{-1} \text{ cm}^{-1}$ for use in determining protein.

G. SPECTRAL MEASUREMENTS

Absorption spectra were recorded using a Cary 15 spectrophotometer.

Enzyme assays were conducted on a Beckman DU modified with a Gilford Model 220 optical density converter.

Most emission spectra were obtained with an Aminco-Keirs spectroffuoremeter with a high pressure Xenon arc lamp and modified with an EMI 9781 R photomultiplier tube. The emission spectrum of the holotryptophanase-L-ethionine complex was obtained with a component system for higher resolution. The excitation wavelength was selected by a Bausch and Lomb 10 cm grating blazed at 3000 Å in a Bausch and Lomb 500 mm monochromator. A TEW sample holder with collimating lenses was used for the right angle alignment. The emission monochromator was a 750 mm Czerny-Turner spectrometer (SPEX 1711-II) which utilized a 10 cm Bausch and Lomb grating blazed

at 5000 Å. Emission was detected with an EMI 9558 QA photomultiplier tube operated on a Fluke 412B power supply. The system utilized a PAR H-3 lock-in amplifier with reference provided by a light chopper. The amplified emission was displayed on a strip chart recorder.

Nanosecond time resolved fluorescence decay measurements were obtained with a single photon counting apparatus. The nanosecond flash lamp is a thyratron-gated lamp with a typical pulse rate of 35 kHz. The lamp is detected with a 1P28 photomultiplier tube and the resulting pulse, after discrimination against low level noise (ORTEC Model 436) is used to start the time to amplitude converter (TAC, ORTEC Model 457). Fluorescence photons are detected by a 56DUVP photomultiplier tibe and the resulting pulse is used to stop the TAC.

Lamp pulse and photon counting rates are measured with MONSANTO Model 150A digital counters. Time jitter is eliminated by using an ORTEC Model 463 discriminator. The calibration of the TAC is performed with the ORTEC Model 462 time calibrator.

Output of the system is fed to a NUCLEAR DATA Model 1100 multichannel analyzer. The contents of the multichannel analyzer memory can be displayed on an oscilloscope (HEWLETT-PACKARD Model 130BR) or can be fed to a teletype equipped with tape punch. Communication with the MSU CDC 6500 computer is accomplished by teletype through an acoustic coupler and a digital plotter (HEWLETT-PACKARD Model 7200A).

H. RAPID-SCANNING STOPPED FLOW KINETICS MEASUREMENTS

The instrument used for rapid-scanning stopped flow kinetics studies was specifically designed for enzyme studies by Ho^{56} , based on an earlier system of Papadakis et al. ⁵⁷ Repetitive scan rates of up to 150 scans per second allow observation of processes occurring on a millisecond time scale after an initial dead time of about 6.5 msec. The system is constructed entirely of inert materials and requires only small volumes (typically about 12 ml) in order to protect and conserve precious biological samples.

The light source is a 1000 W Xenon arc lamp. The system utilizes a scanning monochromator with scan rates of 3 to 150 spectra per second. Sample and reference signals proceed through a beam splitting fiber optics line to matched photomultiplier tubes, with the photomultiplier outputs being amplified by a logarithmic amplifier. The sampling system uses a sample-and-hold amplifier and a 12-bit A to D converter. The system is interfaced to a DEC PDP-8/I computer.

Calibration procedures for the system involve collection of the spectra for neutral density filters in order to determine absorbance values. The spectra of holmium oxide and didymium glass are also collected in order to calibrate the wavelength intervals. Calibration data is submitted for analysis to programs on the MSU CDC 6500 computer.

In addition to the software for the control of the acquisition of data, there is available on the PDP-8/I software for the analysis of data that can be used during the experimental session or at a later time. Spectra can be displayed, averaged, or expanded and solvent or infinity spectra subtracted. Time cuts at particular wavelengths can be

implemented. Finally, data can be transferred to the MSU CDC 6500 computer for calibration procedures and a powerful battery of nonlinear regression programs, KINFIT. A compact and elegant display of the results of a rapid-scanning stopped flow 'push' is the absorbance-wavelength-time surface, one of which is shown in Figure 53.

CHAPTER 6

FUTURE WORK

As discussed in Chapter 1, B₆ compounds often have numerous ionic and tautomeric forms. Enzyme bound Schiff's bases are no exception and this fact explains the large amount of computer analysis of the absorption spectra of B₆ compounds in the literature. Johnson and Metzler³, for example, discuss the methodology for resolving enzyme spectra into the spectra of the individual ionic and tautomeric forms and present such a spectral resolution for aspartate aminotransferase. In general, such methods involve a nonlinear least squares fitting of the individual spectra which best reconstitute the overall spectrum.

The absorption spectrum of holotryptophanase could be analyzed by the method described by Johnson and Metzler³. Although objections might be raised to the use of lognormal distributions, the method has the advantage that programs are available. Certain features of the spectra could be used to extract information about the ionic and tautomeric forms present in the enzyme. Spectral forms thus generated might also be useful as inputs into a more sophisticated analysis.

One such analysis is the analysis of kinetic data by the method of principal components. ⁵⁸ Ionic and tautomeric forms of the enzyme as well as reaction intermediates may be obtained by this method. The experiments in which pH or monovalent cation is changed are particularly

good candidates for this analysis because of their relative simplicity.

Similarly, the fluorescence spectrum of holotryptophanase is composed of the spectra of several ionic and tautomeric forms of the enzyme bound Schiff's base and free pyridoxal-P which is necessarily in equilibrium with the enzyme. Several approaches to the analysis of multicomponent fluorescence spectra are reported in the literature.

Weber⁶⁰ discusses a matrix method for the resolution of fluorescence spectra. The necessary data are elements of an array of values of the fluorescence intensity for pairs of excitation and emission wavelengths, mathematical analysis of which results in the number of components present in a mixture.

Warner et al. 61,62 implement the collection of the 'emission-excitation matrix' by means of a video fluorimeter which uses a low light level television sensor. The spectra of the individual components are fitted by a least squares method employing known spectra or a principal component analysis.

O'Harer and Parks⁶³ discuss the technique of selective modulation in which the excitation wavelength is modulated and the corresponding emission is selected by means of a lock-in amplifier. This metod is demonstrated by the authors for mixtures of up to three components.

Wahl and Brochon 64,65 suggest that an analysis of the fluorescence spectrum of a mixture can be accomplished by analysis of fluorescence lifetime data. If each of the components is a single exponential emitter, the mixture will have a decay law with a term for each component of the mixture. The coefficient of each term will be proportional to the concentration of that component and the quantum yield of fluorescence for that component.

Another area for further study is excited state proton transfer. Usually this phenomenon is investigated by experiments in which the solvent or temperature is varied and the rate of proton transfer is measured. These experiments would give ambiguous results in the case of a small molecule embedded in a protein which itself would respond to these changes of parameters and thus cause changes in the environment of the small molecule in an undetermined manner. One could not directly prove the excited state proton transfer hypothesis for holotryptophanase by such experiments.

A possible method of proof is suggested by Stryer 66, who discusses a deuterium isotope effect on the emission of compounds in which excited state proton transfer is known to occur. He interprets the change in spectral shapes for molecules in deuterated media as resulting from changes in rates of proton transfer due to the effect of the deuteron participating in the reaction; changing the rate changes relative proportions of the original form and the proton transferred form and hence the emission. The absence of a deuterium isotope effect cannot be taken as conclusive evidence that there is no excited state proton transfer because even deuteron rates may be fast enough so that equilibrium is established within the lifetime of the excited state. Also, the proton transfer may be internal to the protein, i.e., assisted by a protein residue, and therefore independent of the presence of deuterium in the external medium.

Another method of looking at this question is suggested by Loken et al. 67 who advocate the use of excited state proton transfer as a biological probe. Rates of excited state proton transfer may vary with environment in which a molecule finds itself and therefore, for a small

molecule embedded in a protein, these rates may be used to detect changes of protein conformation.

conformational analysis of pyridoxal-P amino acid Sciff's bases as performed by Weintraub et al. 10 could be extended to the calculations of properties of the absorption spectra as a function of conformational parameters. Also, a positive charge representing a monovalent cation could be incorporated into such calculations. Detailed knowledge of the effects on the absorption spectrum of conformation and a positive charge could be used to answer such questions as whether the enzyme holds the coensyme in one or more preferred conformations and which positions for the monovalent cation are consistent with spectral data. Such information might assist in attempts to model species present at the active site of the enzyme and to unravel the details of the catallytic act.

BIBLIOGRAPHY

- 1. Mahler, H.R., and Cordes, E.H., <u>Biological Chemistry</u>, 2nd ed., Harper and Row Publishers, New York, 1971.
- 2. Elguero, J., Marzin, C., Katritzky, A.R., and Linda, P., The Tautomerism of Heterocycles, Academic Press, New York, 1976.
- 3. Johnson, R.J., and Metzler, D.E., Methods in Enzymology 18A, 433(1970).
- 4. El-Bayoumi, M.A., El-Asser, M., and Abdel-Halim, F., J. Amer. Chem. Soc. 93, 586, 590(1971).
- Metzler, D.E., Cahill, A., Harris, C.M., Likos, J., and Yang, B., Fed.
 Proc. 36, 855(1977).
- 6. Karube, Y., and Matsushima, Y., Chem. Pharm. Bull. 25, 2568(1977).
- Kupfer, A., Gani, V., ans Shaltiel, S., Biochem. Biophys. Res. Comm.
 1004(1977).
- 8. Gami, V., Kupfer, A., and Shaltiel, S., Biochemistry 17, 1294(1978).
- 9. Dentini, M., Perretti, G., and Savino, M., Biopolymers 17, 897(1978).
- 10. Weintraub, H.J.R., Tsai, M.-D., Byrn, S.R., Chang, C.-J., and Floss, H.J., Int. J. Quantum Chem.: Quantum Biol. Symp. No. 3, 99(1976).
- 11. Morosov, Yu.V., Bazhulina, N.P., Cheraskasina, L.P., and Karpeiskii, M. Ya., Biofizika 12, 397(1967).
- 12. Harris, C.M., Johnson, R.J., and Metzler, D.E., Biochim. Biophys. Acta <u>421</u>, 181(1976).
- 13. Savin, F.A., Bazhulina, N.P., and Morosov, Yu.V., Molekulyarnaya Biologiya 2, 674(1973).

- 14. Bazhulina, N.P., Kirpichnikov, M.P., Morosov, Yu.M., Savin, F.A., Sinyavina, L.B., and Florentiev, V.L., Mol. Photochem.6, 367(1974).
- 15. Morosov, Yu.V., Bazhulina, N.P., Cherakashina, L.P., and Karpeiskii, M.Ya., Biofizika 12, 773(1967).
- 16. Bridges, J.W., Davies, D.S., and Williams, R.T., Biochem. J. <u>98</u>, 451(1966).
- 17. Arrio-Dupont, M., Photochem. Photobiol. 12, 297(1970).
- 18. Weller, A., <u>Progress in Reaction Kinetics</u> (G. Porter, ed.), Vol. II, Pergamom Press, London, 1961.
- 19. Arrio-Dupont, M., Biochem. Biophys. Res. Comm. 44, 653(1971).
- 20. Veinberg, S., Steinberg, I.Z., and Shaltiel, S., Metab. Interconvers. Enzymes, Int. Symp., 4th, 44(1975).
- 21. Veinber, S., Shaltiel, S., and Steinberg, I.Z., Israel J. Chem. <u>12</u>, 421(1974).
- 22. Pullman, B., and Pullman, A., Quantum Biochemistry, Interscience Publishers, New York, 1963.
- 23. Roberts, J.D., and Caserio, M.C., <u>Basic Principles of Organic Chemistry</u>, W.A. Benjamin, Inc., Menlo Park, 1964.
- 24. Ivanov, V.I., and Karpeisky, M.Ya., Advances in Enzymology 32, 21 (1969).
- 26. Shaltiel, S., and Cortijo, M., Biochem. Biophys. Res. Comm. 41, 594 (1970).
- 27. Jones, D.C., and Cowgill, R.W., Biochemistry 10, 4276(1971).
- 28. Cortijo, M., Steinberg, I.Z., and Shaltiel, S., J. Biol. Chem. <u>246</u>, 933(1971).
- 29. Snell, E.E., Advances in Enzymology 42, 287(1975).
- 31. Suelter, C.H., Science 168, 789(1970).

- 32. Toraya, T., Nihira, T., and Fukui, S., Eur. J. Biochem. <u>69</u>, 419 (1976).
- 33. Suelter, C.H., and Snell, E.E., J. Biol. Chem. 252, 1852(1977).
- 34. Hogberg-Raibaud, A., Raibaud, O., and Goldberg, M., J. Biol. Chem. 250, 3352(1975).
- 35. Fenske, J.D., and DeMoss, R.D., J. Biol. Chem. 250, 7554(1975).
- 36. Isom, H.C., and DeMoss, R.D., Biochemistry 14, 4291(1975).
- 37. Isom, H.C., and DeMoss, R.D., Biochemistry 14, 4298(1975).
- 38, Morino, Y., and Smell, E.E., J. Biol. Chem. 242, 2800(1967).
- 39. Snell, E.E., and DiMari, S.J., The Enzymes, Vol. 2, 3rd ed., P.D. Boyer, ed., Academic Press, New York, 1970.
- 40. Suelter, C.H., Wang, J., and Snell, E.E., Anal. Biochem. <u>76</u>, 221 (1976).
- 41. McRae, E.G., Spectrochim. Acta 12, 192(1958).
- 42. June, D.S., personal communication.
- 43. Lewis, C., Ware, W.R., Doemeny, L.J., and Nemzek, T.L., Rev. Sci. Instr. 44, 107(1973).
- 44. Ware, W.R., Doemeny, L.J., and Nemzek, T.L., J. Phys. Chem. <u>77</u>, 2038(1973).
- 45. Lyke, R.L., and Ware, W.R., Rev. Sci. Instr. 48, 320(1977).
- 46. Grinvald, A., and Steinberg, I.Z., Anal. Biochem. 59, 583(1974).
- 47. Knight, A.E.W., and Selinger, B.K., Spectrochim. Acta <u>27A</u>, 1223 (1971).
- 48. Gafni, A., Modlin, R.L., and Brand, L., Biophys. J. 15, 263(1975).
- 49. Britten, A., and Lockwood, G., Mol. Photochem. 2, 79(1976).
- 50. Wong, D.K., and Halpern, A.M., Photochem. Photobiol. 24, 609(1976).
- 51. Rayner, M., McKinnon, A.E., Szabo, A.G., and Hackett, P.A., Can.

- J. Chem. 54, 3246(1976).
- 52. McKinnon, A.E., Szabo, A.G., and Miller, D.R., J. Phys. Chem. 81, 1564(1977).
- 53. June, D.S., Kennedy, B., Pierce, T.H., Elias, S., Halaka, F., Beh-bahani-Nejad, I., El Bayoumi, A., Suelter, C.H., and Dye, J.L., J. Amer. Chem. Soc. 101, 2218(1979).
- 54. Shaltiel, S., and Er-el, Z., Proc. Nat. Acad. Sci. (U.S.) 70, 778 (1973).
- 56. Ho, G.-H., Dissertation, Michigan State University, 1976.
- 57. Papadakis, N., Coolen, R.B., and Dye, J.L., Anal. Chem. <u>47</u>, 1644 (1975).
- 58. Cochran, R.N., Dissertation, Michigan State University, 1977.
- 59. Coolen, R.B., Papadakis, N., Avery, J., Enke, C.G., and Dye, J.L., Anal. Chem. 47, 1649(1975).
- 60. Weber, G., Nature 190, 27(1961).
- 61. Warner, I.M., Callis, J.B., Davidson, E.R., and Christian, G.D., Clin. Chem. 22, 1483(1976).
- 63. O'Haver, T.C., and Parks, W.M., Anal. Chem. 46, 1886(1974).
- 64. Wahl, Ph., and Auchet, J.C., Biochim. Biophys. Acta 285, 99(1972).
- 65. Wahl, Ph., and Brochon, J.C., in C. Sadron, ed., <u>Dynamic Aspects</u>
 of <u>Conformational Changes in Biological Macromolecules</u>, D. Reidel
 Publishing Co., <u>Dordrecht-Holland</u>, 1973.
- 66. Stryer, L., J. Amer. Chem. Soc. 88, 5708(1966).
- 67. Loken, M., Hayes, J., Gohlke, J., and Brand, L., Biochemistry 11, 4779(1972).
- 68. Fasella, P., Turano, C., Giartozio, A., and Hammady, I., Ital. J. Biochem. 10, 174(1961).

